# Relaxation and recombination in spin-polarized atomic hydrogen

D. A. Bell,* H. F. Hess, G. P. Kochanski, S. Buchman, L. Pollack, Y. M. Xiao, D. Kleppner, and T. J. Greytak

*Department of Physics and Center for Materials Science and Engineering, Massachusetts Institute of Technology, Cambridge, Massachusetts 02139*

(Received 7 June 1985; revised manuscript received 7 July 1986)

We have studied relaxation and recombination processes in compressed, doubly polarized atomic hydrogen at temperatures from 0.13 to 0.60 K and magnetic fields from 3 to 9 T. The gas and surface dipole three-body recombination rate constants at a field of 7.6 T are measured to be, respectively, $L_g = 8.9(8)\times 10^{-39}$ cm$^6$s$^{-1}$ and $L_s = 1.2(4)\times 10^{-24}$ cm$^4$s$^{-1}$. They decrease slowly with field and $L_s$ exhibits no significant angular dependence. The three-body recombination rate due to hyperfine mixing has also been measured. Electronic and nuclear relaxation rates have been measured; the $b$-$c$ electronic relaxation rate constant in the gas is $G^{bc} = 1.03(7)\times 10^{-15}$ cm$^3$s$^{-1}$exp$(-E_{bc}/k_B T)$. The temperature and field dependence of the nuclear relaxation rate in the gas are observed to be in excellent agreement with recent theoretical calculations. Three-body surface recombination-rate measurements using $^3$He-$^4$He surfaces indicate that as little as one monolayer of $^3$He on the liquid $^4$He surface appreciably decreases the adsorption energy of atomic hydrogen. Densities achieved include $4.5\times 10^{18}$ atoms cm$^{-3}$ at 0.55 K (pure $^4$He walls), and $1.4\times 10^{18}$ atoms cm$^{-3}$ at 0.19 K (8 at. % $^3$He).

## I. INTRODUCTION

The quest to achieve high densities of spin-polarized atomic hydrogen H↓ has advanced through several relatively well defined stages. In the first observation by Silvera and Walraven,[1] H↓ was detected at particle densities less than $10^{15}$ cm$^{-3}$; this density was rapidly increased to over $10^{16}$ cm$^{-3}$ through technical improvements.[2,3] The limiting factor in these early experiments turned out to be electron depolarization due to hyperfine mixing in one of the two nuclear spin states of the confined species. This process led to a two-body recombination reaction of atoms adsorbed on the liquid helium surface.[4,5] Next, Cline, Greytak, and Kleppner[6] demonstrated that a high nuclear polarization could be achieved in the gas by the spontaneous selective recombination of atoms in the mixed hyperfine state, a process first suggested by Statt and Berlinsky.[7] This creation of doubly polarized hydrogen, H↓↓, opened the way to higher densities at which three-body process predicted by Kagan, Vartanyantz, and Shlyapnikov[8] (KVS) could be investigated.

H↓ has now been studied at densities over $10^{18}$ cm$^{-3}$ by two approaches. Sprik *et al.*[9] compressed a bubble of H↓ in liquid $^4$He; Hess *et al.*,[10] in the first stages of the research to be reported here, used a piston to compress the gas into a small chamber. Both groups detected three-body recombination.

This paper presents the results of an extensive study of decay mechanisms, in particular three-body recombination, in spin-polarized hydrogen. Background information relevant to this research is provided in Sec. II. (A comprehensive account of earlier research on H↓ can be found in a review article by Greytak and Kleppner.[11]) Section III presents a description of the apparatus and the techniques. In Sec. IV the experimental procedure is described; in Sec. V various considerations involved in interpreting the data are discussed. Section VI presents experimental results for the various rate coefficients. The conclusions are summarized in Sec. VII and Table II. A glossary of symbols is provided in Appendix D. Some of this material has appeared earlier in brief form.[12–14]

## II. BACKGROUND

### A. Hyperfine state structure

The hyperfine states of hydrogen in its ground electronic state are usually labeled alphabetically in order of increasing energy. In terms of electron and proton spin eigenstates, the state vectors are

$$\begin{aligned} |a\rangle &= \cos\theta\,|-\tfrac{1}{2},\tfrac{1}{2}\rangle - \sin\theta\,|\tfrac{1}{2},-\tfrac{1}{2}\rangle\ , \\ |b\rangle &= |-\tfrac{1}{2},-\tfrac{1}{2}\rangle\ , \\ |c\rangle &= \cos\theta\,|\tfrac{1}{2},-\tfrac{1}{2}\rangle + \sin\theta\,|-\tfrac{1}{2},\tfrac{1}{2}\rangle\ , \\ |d\rangle &= |\tfrac{1}{2},\tfrac{1}{2}\rangle\ . \end{aligned} \tag{1}$$

$|m_s, m_I\rangle$ denotes the projections of the electron and proton spins along the magnetic field. The mixing angle $\theta$ is given by

$$\tan(2\theta) = \frac{a}{h(\gamma_e+\gamma_p)B} = \frac{0.05061}{B}\ , \tag{2}$$

where $a$ is the hydrogen hyperfine constant, $\gamma_e$ and $\gamma_p$ are the electron and proton gyromagnetic ratios, respectively, and $B$ is the magnetic field in tesla.

At a field of 8 T, the upper two hyperfine states $c$ and $d$ are separated from the lower ones $a$ and $b$ by approximately $2\mu_B B$, an energy corresponding to a temperature 10.7 K. However, at this field the splitting between $a$ and $b$ is only 50.4 mK and between $c$ and $d$ it is only 17.7 mK. In a high field the equilibrium fraction of atoms in

 

the upper two hyperfine states is approximately

$$F_{\uparrow}=\frac{n\uparrow}{n\uparrow+n\downarrow}=e^{-2\mu_B B/k_B T} . \tag{3}$$

The term "spin-polarized hydrogen" generally describes hydrogen under conditions in which $F_{\uparrow}$ is close to zero. For instance, at a temperature of 0.3 K and a magnetic field of 8 T, $F_{\uparrow}=3\times10^{-16}$.

The stability of a gas of atomic hydrogen is limited by the electron polarization $P_e=p_{1/2}-p_{-1/2}$, where $p_m$ is the probability that $m_s=m$. The electron polarizations of the hyperfine states are

$$\begin{aligned} P_e(a)&=-1+2\sin^2\theta \\ P_e(b)&=-1 \\ P_e(c)&=+1-2\sin^2\theta \\ P_e(d)&=+1 . \end{aligned} \tag{4}$$

At temperatures of a few hundred millikelvin and magnetic fields greater than a few tesla, $n_a=n_b=n/2$, and $n_c=n_d=0$. Under such conditions, the average polarization is $P_e=-1+\sin^2\theta$. The "impurity" factor, $\sin^2\theta$, provides a channel for singlet state collisions and direct recombination. However, if only $b$ state atoms are present, both the nuclear and the electronic polarization are exactly $-1$. A gas of such atoms is known as doubly polarized hydrogen, and is denoted by H↓↓.

### B. "Two-body" recombination

It is useful to distinguish recombination processes phenomenologically in terms of the density dependence of the decay rate. Processes which cause the density to evolve as

$$\dot{n}\propto -n^2 \tag{5}$$

are described as *two body,* or *second order,* while processes which obey

$$\dot{n}\propto -n^3 \tag{6}$$

are *three body,* or *third order.* Simple exponential decay can also occur

$$\dot{n}\propto -n . \tag{7}$$

This *one-body* or *first-order* process arises from spurious effects such as leakage of hydrogen atoms out of the storage cell or depolarization by magnetic impurities on the walls. In this paper we adopt the convention that time derivatives indicated by a "dot" above the variable indicate contributions to the total derivative of the process by terms explicitly displayed, as in Eqs. (5)–(7). Total time derivatives, including all relevant processes, will always be indicated by $d(\ )/dt$.

The maximum density of H↓ that can be achieved is ultimately limited by molecular recombination processes. Because there are no bound states of the molecular triplet potential, recombination requires either an intrinsic singlet component in the pair wave function or some process to induce triplet-singlet transitions. Hyperfine mixing in the $a$ state, as discussed above, can lead to the first type of recombination. [KVS (Ref. 8) refer to this as "exchange recombination."] As will be discussed in Sec. II E, the second situation can also occur, notwithstanding the large energy barrier that usually forbids electron spin-flip transitions in a high magnetic field.

The most elementary recombination process is of the form

$$\mathrm{H}+\mathrm{H}+X\rightarrow \mathrm{H}_2+X+D_0 \tag{8}$$

where $X$ represents a third body: another H atom, an impurity such as He, or a surface. $D_0$ is the $H_2$ dissociation energy, 4.48 eV. Even when H↓ is confined in a chamber lined with liquid helium, surface recombination is often the dominant decay mechanism, at least in singly polarized hydrogen.

The surface density $\sigma$ decays according to[4]

$$\dot{\sigma}=-K_s\sigma^2 , \tag{9}$$

where the surface two-body recombination rate constant is

$$K_s=\langle l\rangle v_s . \tag{10}$$

Here $\langle l\rangle$ is an effective "cross length" for surface recombination collisions, ($\langle l\rangle$ depends on the relative spin state of the two electrons), $v_s=(\pi k_B T/M)^{1/2}$ is the mean relative surface speed, and $M$ is the atomic mass.

At low densities where quantum effects and interatomic interactions can be neglected,

$$\sigma=n\Lambda(T)e^{E_b/k_B T} . \tag{11}$$

$E_b$ is the binding energy of hydrogen to the surface—about 1 K for a $^4$He surface—and $\Lambda$ is the thermal de Broglie wavelength

$$\Lambda(T)=(2\pi\hbar^2/Mk_B T)^{1/2} . \tag{12}$$

Assuming that the volume and surface densities stay in equilibrium [so that $V(dn/dt)=A(d\sigma/dt)$, where $V$ is the volume, $A$ is the surface area and $\sigma$ is given by Eq. (9)] the effective two-body volume recombination rate constant due to surface recombination is

$$K=-\frac{1}{n^2}\frac{dn}{dt}=K_s\frac{A}{V}\Lambda(T)^2 e^{2E_b/k_B T} . \tag{13}$$

The recombination rate depends on which two of the four hyperfine states are involved, and is denoted by $K_{\alpha\beta}$ where $\alpha,\beta$ stand for $a$, $b$, $c$, or $d$ states, and $\delta$ is the Kronecker delta:

$$-\dot{n}_\alpha=\sum_{\substack{\beta,\gamma=\{a,b,c,d\}\\ \beta\le\gamma}} K_{\beta\gamma}n_\beta n_\gamma(\delta_{\alpha\beta}+\delta_{\alpha\gamma}) . \tag{14}$$

For zero nuclear polarization, i.e., $n_a=n_b=n/2$, and complete electron polarization,

$$K=-\frac{1}{n^2}\frac{dn}{dt}=\tfrac{1}{2}(K_{aa}+K_{ab}) . \tag{15}$$

($K_{bb}=0$ since a $b$-$b$ collision is in a pure triplet state.)

The experimental signatures of two-body surface recombination are the temperature dependence of the decay constant $K$, $T^{-1/2}\exp[2E_b/k_B T]$, and its dependence on magnetic field, $B^{-2}$. The field dependence arises be-

cause at high fields the probability of finding an $a$ atom in the $m_s=\frac{1}{2}$ state is the square of the hyperfine mixing angle $\theta$, and $\theta$ is proportional to $B^{-1}$ at high fields [see Eq. (2)]. At $B=8$ T and $T=0.3$ K we have measured $K_s=5.1(3)\times10^{-10}$ cm$^2$ s$^{-1}$ and $E_b/k=1.01(6)$ K for a sample consisting of approximately equal numbers of $a$ and $b$ atoms.[15] These values are typical of those measured by other groups,[5,16,17] although there is some spread in the values reported for $K_s$. In an unpublished experiment[18] we have obtained $\gamma\equiv K_{aa}/K_{ab}=2.8(4)$ at $T=0.3$ K and $B=8$ T. Again, this is typical of values found by other groups.[16,17,19,20]

Equation (14) can be integrated for a sample in which $c$ and $d$ atoms can be neglected to show that after the $a$ atoms have all recombined, a sizeable fraction of $b$ atoms remain.

We have followed the theory of Greben, Thomas, and Berlinsky[21] and parametrized the two-body recombination constants as follows:

$$\begin{aligned}
K_{aa}&=\tfrac{1}{2}K_p\sin^2\theta\cos^2\theta\ ,\\
K_{ab}&=\tfrac{1}{2}K_o\sin^2\theta\ ,\\
K_{ac}&=\tfrac{1}{4}K_p(\cos^2\theta-\sin^2\theta)^2+\tfrac{1}{4}K_o\ ,\\
K_{ad}&=\tfrac{1}{2}K_o\cos^2\theta\ ,\\
K_{bb}&=0\ ,\\
K_{bc}&=\tfrac{1}{2}K_o\cos^2\theta\ ,\\
K_{bd}&=\tfrac{1}{4}K_p+\tfrac{1}{4}K_o\ ,\\
K_{cc}&=\tfrac{1}{2}K_p\sin^2\theta\cos^2\theta\ ,\\
K_{cd}&=\tfrac{1}{2}K_o\sin^2\theta\ ,\\
K_{dd}&=0\ .
\end{aligned}\tag{16}$$

$K_o$ and $K_p$ are constants specifying recombination rates into orth-$H_2$ and para-$H_2$, respectively, and $\theta$ is the hyperfine mixing angle [Eq. (2)]. If there were no other decay mechanisms in spin-polarized hydrogen, once the $a$ atoms had recombined, the remaining gas of electron and nuclear polarized hydrogen, H↓↑, would be stable. This, however, is not the case.

### C. Spin relaxation

Although a gas of pure $b$ state atoms is stable against recombination, nuclear relaxation can occur during collisions, transferring atoms into other states which promptly recombine on the surface by colliding with $b$ atoms. The atoms experience fluctuating magnetic fields due to the electronic magnetic moments of passing hydrogen atoms. The relaxation rate is proportional to the total collision rate, thus the relaxation equations have the form

$$-\dot{n}_\alpha=\sum_{\substack{\beta,\gamma,\theta,\sigma\\ \beta\le\gamma,\ \theta\le\sigma}} G_{\beta\gamma,\theta\sigma}n_\beta n_\gamma(\delta_{\alpha\beta}+\delta_{\alpha\gamma}-\delta_{\alpha\theta}-\delta_{\alpha\sigma})\tag{17}$$

where $\alpha,\beta,\gamma,\theta,\sigma$ represent arbitrary hyperfine states, and $G_{\beta\gamma,\theta\sigma}$ is the rate constant for the process $\beta+\gamma\rightarrow\theta+\sigma$. Following previous usage, we observe that $G_{bb,ab}=G_{ab,aa}$ (Ref. 22) and define the nuclear relaxation rate $G^{ba}\equiv G_{bb,ab}=G_{ab,aa}$. If $G^{ba}\ll K$, a quasi-stationary state is achieved in which recombination is limited by nuclear relaxation. This relaxation bottleneck gives rise to a decay of the form

$$\dot{n}\approx-2G^{ba}\left[1-\gamma\frac{G^{ba}}{K_{ab}}\right]n^2\ .\tag{18}$$

The nuclear polarization in this situation is

$$P_n=\frac{n_a-n_b}{n_b+n_a}\approx-1+\frac{2G^{ba}}{K_{ab}}-(\gamma-\tfrac{1}{2})\left[\frac{2G^{ba}}{K_{ab}}\right]^2\ .\tag{19}$$

That slow nuclear relaxation would govern the decay of H↓↑ was predicted by Statt and Berlinsky,[7] and first observed by Cline, Greytak, and Kleppner.[6]

Theoretical calculations by van den Eijnde[23] give the following expression for the nuclear relaxation rate constant in the gas:

$$G_g^{ba}=\left[6.33\times10^{-22}T^{1/2}+7.57\times10^{-22}\frac{E_{ab}}{k}T^{-1/2}\right]F(B)\ \text{cm}^3\,\text{s}^{-1}\ ,\tag{20a}$$

$$F(B)\equiv\left[\frac{\gamma_p+\sin\theta\gamma_e}{\gamma_p}\right]^2\approx\left[1+\frac{16.68}{B}\right]^2\ ,\tag{20b}$$

where $E_{ab}$ is the energy difference between the lowest two hyperfine states and $B$ is the magnetic field in tesla. The field-dependent factor $F(B)$ in the equation is common to all expressions for nuclear relaxation; it is the square of the ratio of the effective perpendicular moment of the polarized hydrogen atom to the nuclear moment.

Nuclear relaxation can occur on surfaces as well as in the bulk gas. $G_s^{ba}$ has been predicted to depend strongly on the surface orientation, vanishing when the normal to the surface is parallel to the magnetic field[24–27] and having a maximum when the normal is near 45° to the field. Using the results of a more recent calculation,[28] evaluated $T=0.3$ K,

$$G_s^{ba}(45°)=8\times10^{-15}F(B)\ \text{cm}^2\text{s}^{-1}\ ,\tag{21}$$

which can be converted to an effective bulk rate using the arguments that let to Eq. (13).

Nuclear relaxation has been studied experimentally by three groups.[6,16,19] The bulk rate $G_g^{ba}$ agreed with theory[7,23,29] (and more measurements will be reported in this article), but the measured surface rate $G_s^{ba}$ was 50 times too large. As explained in Appendix B, measurements made in our compression apparatus indicate that this was due to a misinterpretation of the cause of the surface associated decay.[12]

An important parameter in many experiments is the ratio $G^{ab}/(K_{ab}+K_{aa})$. In the absence of surface relaxation this ratio can be estimated by using for $G$ the leading term in Eq. (20a) and for $K$, Eq. (13) with our value of $K_s=5.1\times10^{-10}$ cm$^2$ s$^{-1}$ measured at $B=8$ T and $T=0.3$ K. The magnetic field dependence of $G$ [Eq. (20b)] is nearly canceled by the field dependence of $K_s$ ($\propto B^{-2}$), so the estimate

$$G^{ab}/(K_{aa}+K_{ab})=1\times10^{2}(V/A)Te^{-2E_b/k_BT} \quad (22)$$

is valid under the conditions which pertain in these experiments.

### D. Electronic relaxation

The fluctuating magnetic field due to the electronic moments of mobile neighbors can also induce electronic relaxation. During a collision, a $b$-state atom can be promoted to the $c$ state by this process. Most of these $c$-state atoms will recombine with a $b$-state atom (see Appendix A), giving rise to a two-body contribution to the decay.

$$\dot{n}=-2G^{bc}n^{2}, \quad (23)$$

where we define $G^{bc}\equiv G_{bb,bc}=G_{ad,dd}=G_{aa,ad}=G_{bc,cc}$. The electronic relaxation rate constant $G^{bc}$ is expected to differ from the nuclear rate constant $G^{ba}$ in at least two respects: it will be larger by the square of the ratio of electronic moment to the effective nuclear moment, and it will be smaller by the Boltzmann factor describing the probability that the incoming atoms have sufficient kinetic energy to flip the electronic spin. The Boltzmann factor prevents this process from being important at high magnetic fields and low temperatures. $G^{bc}$ can be expressed as

$$G^{bc}=G^{cb}e^{-E_{bc}/k_BT}, \quad (24)$$

where $G^{cb}$ is the coefficient for the inverse processes to $G^{bc}$. A calculation by KVS (Ref. 8) yields $G^{cb}=2\times10^{-15}$ cm$^3$ s$^{-1}$.

Electronic relaxation in H↓ was first observed by Sprik, Walraven, and Silvera.[9] Additional measurements are presented in Sec. VI A of this paper.

There are other relaxation mechanisms which can transform $c$ state atoms produced by a three-body recombination before the atoms recombine. For $T\geq0.6$ K, this can lead to incorrect values of rate constants unless the analysis explicitly includes both the $c$ and $d$ states. This problem is discussed in Sec. V B 5.

### E. Three-body recombination

At high densities, H↓ is destroyed predominantly by three-body processes, either in the bulk or on the surface. Kagan, Vartanyantz, and Shlyapnikov[8] carried out a systematic survey of decay modes in H↓ and pointed out the significance of three-body recombination. This process was later observed experimentally[9,10] and is now regarded as the limiting factor in achieving high density.

In their paper, KVS calculate the rate $W$ of three-body events per atom in the gas. The leading three-body process in singly-polarized H↓ arises from the spin impurity in the $a$ state, much as in two-body surface recombination. KVS refer to this as an "exchange process," although "hyperfine mixing" might be a more suitable term. In their theory at least two of the three atoms must be in the $a$ state. The three-body rate per atom due to exchange in the gas, $W_g^{\rm ex}$, can be written as

$$W_g^{\rm ex}=C_g^{\rm ex}n^{2}[(n_a/n)^3+\tfrac{1}{3}(n_b/n)(n_a/n)^2]. \quad (25)$$

At a field of 10 T, KVS calculate $C_g^{\rm ex}=1\times10^{-37}$ cm$^6$s$^{-1}$. Most experimental scenarios at high densities involve doubly-polarized hydrogen, H↓↓, for which $W_g^{\rm ex}=0$. However, under certain conditions we have been able to measure this rate (see Sec. V B 4).

In doubly polarized hydrogen the major recombination mechanism is a three-body process in which an atom effectively undergoes electronic dipolar spin relaxation, similar to that described in the last section, while simultaneously making a transition to a bound molecular state. In two-body electronic relaxation the magnetic spin-flip energy, $E_{bc}\approx2\mu_BB$, must be provided by the translational kinetic energy, with the result that $G_{bb,bc}$ is suppressed by the Boltzmann factor $\exp[-E_{bc}/k_BT]$. In a three-body collision, however, the spin-flip energy can be provided by the molecular recombination energy. Thus, there is no energy barrier and recombination can occur even in a very high magnetic field or at a very low temperature.

The electron dipole three-body recombination event rate per particle in the gas $W_g^d$ has the form

$$W_g^d=C_g^dn^{2}[(n_b/n)^3+(n_b/n)^2(n_a/n)+(n_b/n)(n_a/n)^2+(n_a/n)^3]. \quad (26)$$

In the zero-temperature limit at a magnetic field of 10 T, KVS calculate $C_g^d=3\times10^{-39}$ cm$^6$s$^{-1}$. They predict that $C_g^d$ should increase by about a factor of 3 between 5 and 10 T.

The KVS theory applies only at $T=0$: the possible temperature dependence of various rates was not calculated. Furthermore, certain recombination channels that are absent at $T=0$, could be important at the highest temperature used in these experiments. An example is the three-body exchange process in which one $a$-state atom and two $b$-state atoms react to form $H_2$ in the ortho state and a $b$-state atom. This gives rise to an additional term in Eq. (25) proportional to $(n_a/n)(n_b/n)^2$, but with a coefficient that KVS show to vanish at $T=0$. A similar process was considered by Greben, Thomas, and Berlinsky[21] in their quantum theory of the recombination reaction of hydrogen in the presence of helium. One of the contributions to $H+H+He\rightarrow H_2+He$ was $a+b+He\rightarrow$ortho-$H_2+He$. This contribution disappears at $T=0$ but dominates the total reaction of unpolarized atoms at $T=1$ K. The process is close to the process $a+b+b\rightarrow$ortho-$H_2+H$ that was neglected by KVS. One can use the Greben *et al.* results to obtain an order of magnitude estimate of the $a+b+b$ contribution to Eq (25); it is $-\dot{n}=(3\times10^{-39}$ cm$^6$s$^{-1}$K$^{-1})Tn_an_b^2$ at a field of $B=7.6$ T. We will return to this point in Secs. V B 4 and V B 5 when we examine high-temperature decays with only modest polarization. Fits of our data with *aab* but without *abb* processes provided somewhat better agreement than fits including the latter but not the former. In the absence of a fully temperature dependent theory, the best that can be done at present is to compare our measured results with the KVS theory for $T=0$.

Three-body recombination also takes place on the surface. The surface does not actively participate in recombination: each of the three bodies must have a spin. Although the mechanisms for recombination on the surface

and in the gas are essentially the same, the surface and the bulk rates differ because of the closer proximity of the hydrogen atoms on the surface due to adsorption, and the somewhat modified dynamics and final state density due to the two-dimensional structure of the surface film. Kagan, Shlyapnikov, Vartanyantz, and Glukhov[30] argue that these considerations allow the surface rate to be expressed in terms of the volume rate and a characteristic localization distance perpendicular to the surface $l=5$ Å.

$$C_s^d=\frac{4}{3l^2}C_g^d . \tag{27}$$

A recent calculation by de Goey *et al.*[31] indicates that the relation between $C_s^d$ and $C_g^d$ may be more complex than indicated by Eq. (27).

The electron dipole three-body rate for H↓, $W^d$, is not the same as the atomic loss rate since each electron spin-flip transition can cause the loss of several atoms. In the initial three-body event, two of the atoms form a molecule and are lost from the system. We refer to this as *prompt* recombination. If the atom that is expelled from the initial event maintains its original electron spin state, it plays no further role. However, if the expelled atom has had its electron spin flipped, it will give rise to a *delayed* recombination which removes an additional two atoms from the system. (This assumes that the expelled atom recombines before its electronic spin can relax back to its equilibrium state; we show in Appendix A that this is true at all but our highest temperature.) Thus, the three-body rate coefficients in the gas, $C^{\alpha\beta\gamma}$ are defined by

$$-\dot{n}_\theta=\sum_{\substack{\alpha,\beta,\gamma=\{a,b,c,d\}\\ \alpha\le\beta\le\gamma}} C^{\alpha\beta\gamma}(\delta_{\alpha\theta}+\delta_{\beta\theta}+\delta_{\gamma\theta}-N^{\alpha\beta\gamma\theta}) . \tag{28}$$

$C^{\alpha\beta\gamma}$ is the rate constant for the event rate, and $N^{\alpha\beta\gamma\theta}$ is the number of $\theta$ state atoms produced in an $\alpha+\beta+\gamma$ recombination.

From Eqs. (25) and (26), it can be seen that $C^{aaa}=C^{ex}+C^d$; $C^{aab}=\frac{1}{3}C^{ex}+C^d$, and $C^{bbb}=C^{abb}=C^d$. When the temperature is sufficiently low for all $c$ or $d$ atoms to recombine immediately, then

$$L_g=\frac{1}{n^2}(2+2N^d)W_g^d=(2+2N^d)C_g^d , \tag{29}$$

where in the KVS theory, $N^d=N^{\alpha\beta\gamma c}+N^{\alpha\beta\gamma d}$ independent of $\alpha,\beta,\gamma$ in the set $\{a,b\}$. $N^d$ is the fraction of three-body dipole-dipole processes that leave the unrecombined atom in the $c$ and $d$ states. [The parameter $\lambda$, introduced in our previous publications, Refs. 10 and 12–14, is related to $N^d$ by $\lambda=2(1+N^d)$.]

The atom ejected by three-body recombination is calculated to be in the $c$ or $d$ state 93% of the time.[8] At 0.6 K in our experiment a fraction of the $c$ or $d$ atoms can relax back down to the $a$ or $b$ state before themselves recombination state reducing the observed value of $L$ by perhaps 30%.

Similar expressions can be found for the three-body rate coefficient on the surface $L_s$:

$$\dot{\sigma}=-L_s\sigma^3 , \tag{30}$$

$$L_s=\frac{1}{\sigma^2}(2+2N_s^d)W_s^d=(2+2N_s^d)C_s^d . \tag{31}$$

As with $K$ and $G$, one can define an effective volume contribution to $L$ due to the surface term.

$$L=L_g+L_{\text{eff}} , \tag{32}$$

$$L_{\text{eff}}=\frac{A}{V}L_s(\sigma/n)^3=\frac{A}{V}L_s[\Lambda(T)e^{E_b/k_BT}]^3 . \tag{33}$$

The three-body rate coefficient $L$ is of central importance since it is this quantity which is measured directly in these experiments. The strong temperature dependence of $L_{\text{eff}}$ makes it easy to separate the gas and surface contributions to $L$. We will see that the surface contribution is dominant at the lowest temperatures used in these experiments, while at higher temperatures it plays only a minor role.

### F. Decay of H↓↕

To study hydrogen at high densities, it is desirable to use doubly polarized hydrogen, for this is most stable against recombination. The evolution of the density is fundamentally governed by two-body relaxation and three-body recombination:

$$\frac{dn}{dt}=-2Gn^2-Ln^3 . \tag{34}$$

Below 0.6 K, $G$ can be approximated as the sum of the two relaxation rates:

$$G=G^{ba}+G^{bc} . \tag{35}$$

$L$ is given by Eqs. (32) and (33). Although Eq. (34) represents a simplified description of the evolution of the gas, it provides a straightforward method for extracting decay constants from the data that is accurate in certain regimes. However, a more detailed description is required to take into account possible effects such as heating and incomplete polarization that can cause the evolution to deviate from Eq. (34). Such a description is presented in Sec. V.

## III. APPARATUS AND TECHNIQUES

Early experiments on H↓ employed an open cell geometry in which the maximum density is determined by a balance between the flux $f$ of atoms filling the cell and the effective two-body recombination rate $K$:

$$n_{\max}=\left[\frac{f}{KV}\right]^{1/2}\propto\left[\frac{f}{A}\right]^{1/2} . \tag{36}$$

The second expression follows because $K$ is proportional to the area-to-volume ratio. Attempts to increase $n_{\max}$ by increasing the flux become self-defeating. The recombination heating rate increases with $f$; removing the heat requires increasing the surface area, but as Eq. (36) reveals, this tends to reduce $n_{\max}$. Furthermore, increasing the flux-to-area ratio by 100 increases $n_{\max}$ only by a factor of 10. At higher densities where three-body recombination is important, the improvement in $n_{\max}$ with $f/A$ is even less.

The approach that we have used was developed together with R. W. Cline. A sample of doubly polarized hydro-

gen produced by previous techniques[6] is mechanically compressed by a solid piston into a small pancake-shaped volume. The $a$-state atoms are eliminated by recombination before and during the compression; the large $A/V$ ratio facilitates heat removal. Consequently, the final density is not flux limited.

Figure 1 shows a schematic diagram of the low temperature apparatus. Molecular hydrogen from a room temperature gas handling system flows into the liquid nitrogen cooled discharge at constant pressure. From the discharge, atomic hydrogen passes through the refrigerator. Atoms with the correct electron spin are pulled into the high-field region and enter an experimental cell. The cell walls are coated with a saturated layer of superfluid helium to minimize surface adsorption and to provide a seal around the piston. The hydrogen is then compressed into the small fixed volume sample chamber. The temperature and pressure of the gas are recorded during the subsequent decay of the gas density in the sample chamber.

### A. Dissociator

The dissociator is shown in Fig. 2; it consists of a helical resonator driven with about 10 W of power at 50 MHz. The resonator is immersed in liquid nitrogen to improve the $Q$ of the cavity and remove the generated heat. An orifice of diameter 1–2 mm at the bottom of the 11-mm o.d. Pyrex discharge tube provides an impedance to the flow of the gas and allows its pressure to be controlled by a piezoelectric valve in the gas handling system. The discharge intensity is monitored through a Balmer $\alpha$-line filter by a photodiode that is mounted at the top of the glass tube at room temperature.

After leaving the dissociator through the orifice, the gas enters the cross arm where any undissociated molecular hydrogen freezes out on the walls. The cross arm, insulated from the 4.2 K helium bath, is heated in order to decrease the adsorption time (and associated recombination) of the atomic hydrogen on the molecular-hydrogen-coated walls. A temperature of approximately 10 K gives best results.

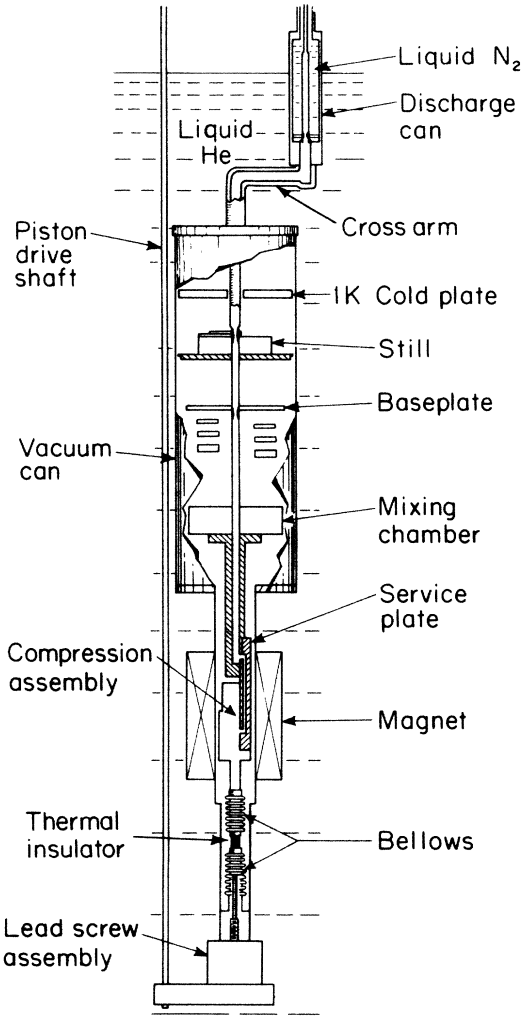


FIG. 1. Schematic diagram of apparatus for compression experiments in spin-polarized hydrogen.

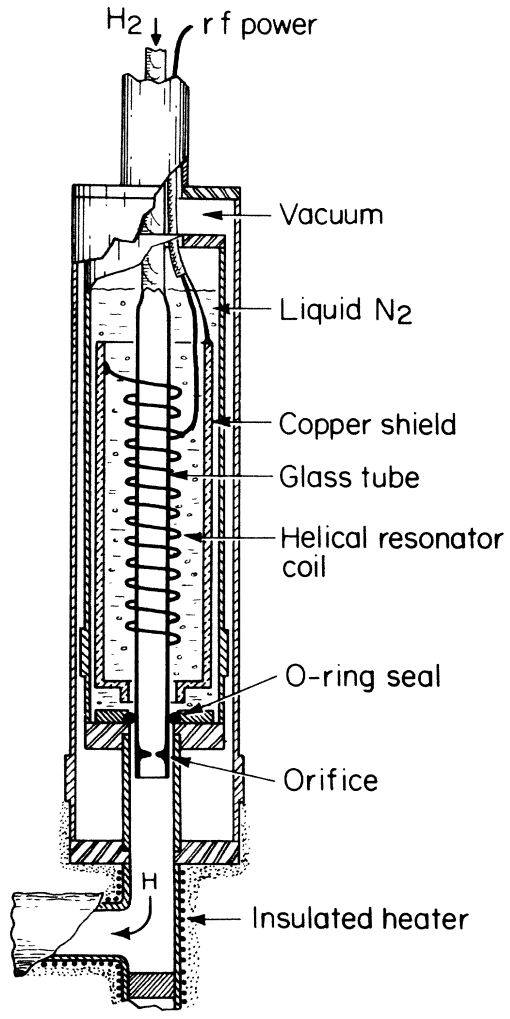


FIG. 2. Liquid-nitrogen temperature dissociator. The entire assembly shown in the figure is immersed in the 4-K liquid-helium bath.

### B. Cooling the hydrogen

The experiment uses a S.H.E. Corp. Model 430 dilution refrigerator with a cooling power of 2 mW at 0.3 K. The atomic hydrogen flows down through the refrigerator in a straight tube located on axis, as indicated in Fig. 1. The tube is maintained at about 10 K down to a 3-cm-long transition region located just above the still. Below the transition region the inside walls of the tube are coated with superfluid $^4$He. The film is thermally anchored to the still by a sintered copper heat exchanger. The film is also anchored to the refrigerator at the baseplate and the mixing chamber. The heat leak between the mixing chamber and the still caused by superfluid helium film flow is limited by the critical velocity of the film $v_c$ (up to 30 cm/s) and the circumference of the tube. The film flows at speeds up to $v_c$ to the warmer parts of the refrigerator where it evaporates; the gas travels back to the colder part and recondenses, releasing a large amount of heat. This problem is reduced substantially by placing 0.3-cm-diam constrictions in the tube at the still and below the baseplate.

The flux of hydrogen atoms that reaches the cell is determined by several factors. The flux generally increases with the temperature of the cross arm, but above about 10 K the refrigerator performance is seriously degraded. When the cell is at low temperature (below 0.15 K), the flux is limited by the cooling power available to maintain temperature control. As long as there is adequate cooling power at the mixing chamber, the flux increases as the still temperature is decreased, perhaps because the effective length of the transition region decreases. A flux of $8\times10^{14}$ atoms $s^{-1}$ measured at the cell, is common. Typically we accumulate $1.5\times10^{17}$ atoms $cm^{-3}$ before turning off the source and letting the gas polarize. However, with our large compression ratio of 110, the density we can attain is limited by the recombination heating after compression, not by the initial flux.

### C. Compression cell

The compression cell assembly is shown in Fig. 3. It is suspended from a service plate consisting of three pieces of oxygen-free high-conductivity copper that are silver soldered together. The hydrogen is transported through a 3-mm hole bored in the service plate. The cell block is firmly bolted to the service plate by six copper screws; an indium o-ring provides a vacuum seal around the hydrogen fill port. The piston assembly, bolted to the bottom of the cell, is also sealed with an indium o-ring. The copper piston slides in a 5.13-mm-diam cylinder with only 3-$\mu$m clearance. The clearance must be smaller than the capillary radius of liquid helium to allow the helium to form a seal between the piston and the walls of the cylinder.

The piston push rod is connected by stainless-steel welded bellows and a Teflon thermal insulator to a lead screw at the very bottom of the vacuum can. The lead-screw mechanism is driven by a shaft which is activated by a computer-controlled stepping motor at room temperature. The maximum vertical motion of the piston is 3 cm; the step size is 5 $\mu$m. A flexible link in the push rod

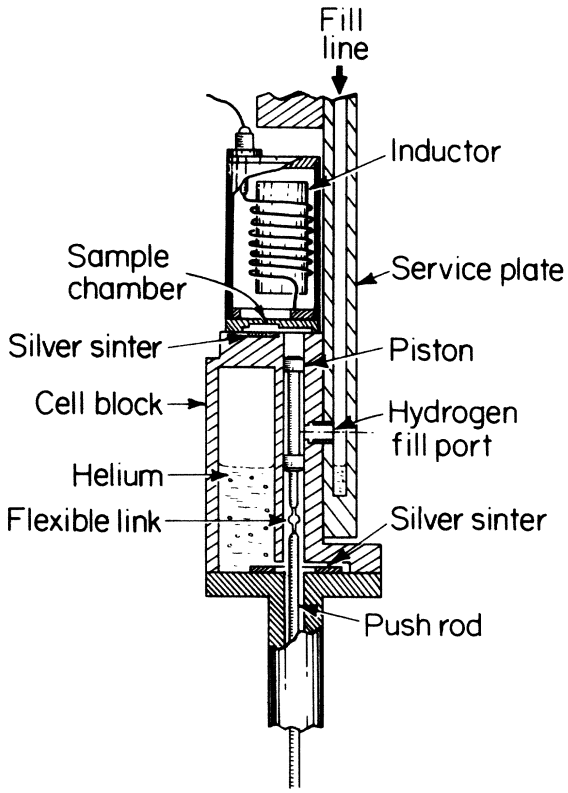


FIG. 3. Compression cell assembly. The piston compresses the H↓ into the disk-shaped sample chamber, which is shown in more detail in Fig. 4.

allows self-alignment of the piston with the cylinder. The position of the piston near the top of the cylinder is determined from the shift in the frequency of the pressure transducer oscillator. This shift is due to the stray capacitance between the piston and the transducer lead above it. When the piston hits the top, the frequency stops changing. A thin Kapton[32] disk was carefully placed on top of the piston to reduce this capacitance.

In addition to sealing the piston, the superfluid helium coating serves to separate the atomic hydrogen from magnetic impurities which may be on the wall. The helium film thickness $t$ at height $h$ above the helium puddle is given by[33]

$$t=\frac{4\times10^{-6}}{h^{1/3}}\ \text{cm}\ , \tag{37}$$

where $h$ is in cm. However, if frozen gas is present this underestimates the thickness by as much as a factor of 3.[33] Thus, accumulation of molecular hydrogen on the surfaces could significantly increase $t$.

Helium has a small but significant surface tension, $\alpha=0.37$ erg $cm^{-2}$, which maintains the piston seal and smooths out any small pits and grooves in the compression chamber. Helium will fill a gap between two parallel plates separated by a distance $d$ at a height $h$ above the liquid level as long as $d$ is less than twice the capillary radius $r$:

$$r=\frac{\alpha}{\rho g h}=\frac{2.6\times10^{-3}\ \mathrm{cm}^2}{h}\ , \tag{38}$$

where $g$ is the gravitational acceleration and $\rho$ is the mass density, equal to 0.145 g cm$^{-3}$. For example, if the largest gap between the piston and cylinder is 5 $\mu$m, then the helium level must be closer than 10 cm below the piston top.

It is desirable to have the helium level remain a constant distance below the top of the piston as the piston moves up. This is accomplished by an auxiliary cylinder which is designed so that that the cross-sectional area for the liquid helium in the cell block is identical to the effective area of the bellows. At the start of a run, liquid helium is added until the piston seals at all vertical positions. Typically 12 cm$^3$ of $^4$He are used, placing the helium level roughly 4 cm below the piston top. When $^3$He is added to reduce the adsorption energy of hydrogen to the surface, the surface tension decreases and it becomes difficult to seal the piston consistently.

To minimize temperature gradients in the compressed sample of hydrogen, a high area-to-volume ratio is desirable. This is the rationale for our "pancake" geometry. This geometry also permits the temperature and pressure of the gas to be monitored easily. Figure 4 shows an exploded view of the sample chamber. To improve heat removal, the lower surface of the cell is composed of 70-nm silver powder which is sintered at high pressure into a depression in the cell block. The upper surface of the cell, facing the sinter, is a pressure transducer consisting of several Kapton[32] layers; gold films evaporated on two of these form the capacitor plates and leads. The diaphragm is 0.64 cm in diameter and 8 $\mu$m thick; the spacing between the transducer plates is about 13 $\mu$m. On the surface of the diaphragm facing the atomic hydrogen are two carbon film thermometers made by spraying Aerodag[34,35] (colloidal graphite) onto evaporated gold contacts. To allow measurement of radial heat gradients, one film thermometer is in the center and the other surrounds it. The Aerodag on the upper surface is flat to approximately 3 $\mu$m as measured by a scanning electron microscope; the surface of the sinter is flat to 1 $\mu$m. For the expected level of the helium, the capillary radius from Eq. (38) is 5–10 $\mu$m, sufficiently large to fill any surface irregularities.

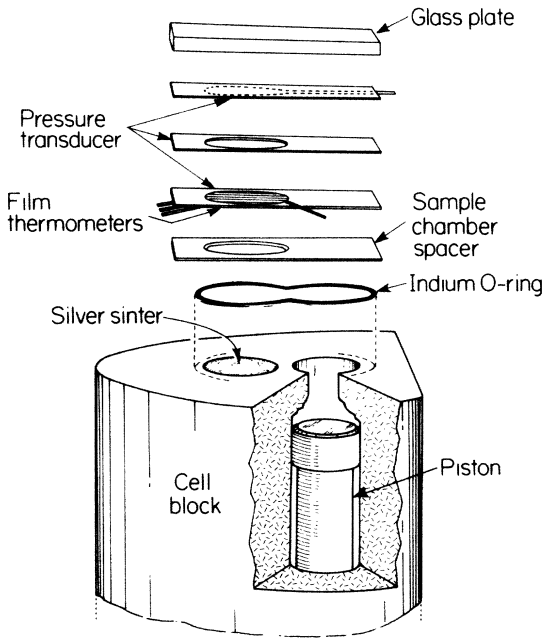


FIG. 4. Exploded view of the sample chamber. The effective height of the sample chamber is 75(10) $\mu$m.

The pressure transducer assembly, backed by a glass slide, is sealed to the top of the cell block by squeezing a 250-$\mu$m wire of indium between them. The cell thickness is determined by the spacer and the indium thickness. The ideal gas law is used to measure the volume of the compression chamber. The pressure of H↓ when the piston is 1 mm below the top is compared to the pressure when it reaches the top. The final volume is found to be $4.3(2)\times10^{-3}$ cm$^3$.

The area of the cell is more difficult to determine. If one assumes that the region directly above the piston is filled with helium by capillary condensation, the horizontally oriented area is 1.1(1) cm$^2$, which is much larger than the vertically oriented area of 0.040(2) cm$^2$. The total area to volume ratio is then 270(30) cm$^{-1}$. The distance between the film thermometers and the sinter is 90(10) $\mu$m at the center of the cell, but is slightly smaller at the edges.

The magnetic field is produced by an uncompensated American Magnetics Corp. 8-T superconducting solenoid which, if cooled to near the helium $\lambda$ point, can be operated at 9 T. The magnetic field varies by $1.5\times10^{-2}$ T across the diameter of the cell, uniform enough to insure that the pressure of hydrogen is uniform throughout the cell. Most of the gradient arises because the compression chamber is off axis. This geometry was chosen to allow the piston to be on axis and to facilitate assembly.

### D. Temperature and pressure measurements

Five thermometers are used in the experiment. The cell block thermometer, a Speer carbon resistor, is used to control the temperature of the cell. Two carbon film thermometers are used to monitor the temperature of the hydrogen after compression. These resistance thermometers, measured by standard three- or four-wire lock-in techniques, are calibrated against two standard thermometers located in low magnetic field on the mixing chamber. The first calibration thermometer is a $^3$He melting curve thermometer, usable below 0.3 K, of the type developed by Greywall and Busch.[36] The second is a doped germanium resistor (type GR-200A-100) from Lake Shore Cryotronics, calibrated at and above 0.3 K.

The cell block thermomenter is in the high-field region and a small (few percent) field-dependent correction is required. The absolute accuracy of the cell block thermometer calibration is 2 mK, though a resolution of better than 0.1 mK is achievable. The film thermometers in the compression cell are not quite so stable; their calibration is referenced to the cell block after each hydrogen compression.

The capacitive pressure transducer is calibrated against the vapor pressure of $^4$He after the cell block thermometer has been calibrated. Due to uncertainties in the temperature calibration, the absolute accuracy of the pressure measurements is only 5%. The capacitance of the pressure transducer and an inductor determine the frequency of a tunnel diode oscillator.[37] This frequency is easily measured and is typically stable to two parts in $10^8$ over an hour. Such a stability requires careful rf shielding and filtering of the pressure transducer circuit. The same precautions must be taken for the film thermometers since they are capacitively coupled to the pressure transducer. The noise in the pressure measurement corresponds to fluctuations of approximately $10^{-2}$ dyn cm$^{-2}$.

## IV. PROCEDURE

A typical compression run begins with the sample chamber, piston cylinder and service plate empty, and the piston down. The discharge is started and H↓ is allowed to accumulate until the density reaches about $10^{17}$ atoms cm$^{-3}$. At this stage the gas cannot spontaneously acquire high nuclear polarization except at the lowest temperatures. High polarization requires that the rate of nuclear relaxation (predominantly a bulk process) be much slower than the rate for recombination (a surface phenomenon). The ratio of these two rates depends on the temperature and the volume-to-area ratio. For the piston down configuration, $V/A \approx 0.1$ cm. Using Eqs (19) and (22), the nuclear polarization at 0.3 K is calculated to be $-0.96$; at 0.6 K, however, the polarization is close to zero.

It is essential to achieve high nuclear polarization before attempting to attain high density: otherwise the $a$-state "exchange" contribution to the three-body recombination $W^{ex}$ can heat the gas enough to cause a thermal explosion. The nuclear polarization is increased by compressing the gas in stages, that is, moving the piston upward by predetermined increments. As the piston moves upward the volume-to-area ratio decreases, driving the equilibrium polarization closer to $-1$. This stepwise motion also allows most of the heat generated by the flexing of the bellows to be dissipated before the final compression step. In the final step the piston typically is advanced 3 mm to the top of the cylinder in 6 s. Even with these precautions, however, at the highest temperatures there is evidence of incomplete nuclear polarization. In the worst cases, the sample suddenly recombines. Such "thermal explosions" have been reported in other compression experiments[9,38] and have been discussed by Kagan, Shlyapnikov, and Vartanyantz.[39] Thermal explosions limit the highest temperatures at which we can work to about 0.6 K. Analysis of the data at 0.6 K, as described in Sec. V B, reveals that even after the compression stops the nuclear polarization takes a noticeable time to relax to a value consistent with the very low volume-to-area ratio of the sample chamber.

To achieve complete nuclear polarization at the highest temperatures, we attempted to prepolarize the gas by preparing it at a low temperature and warming to the desired temperature just before the final compression step. This technique was only marginally useful, presumably because the gas was able to relax to its equilibrium (smaller) polarization while the cell's temperature was being raised.

The state of the gas is monitored continuously by recording the pressure in the cell, the temperatures at the two thermometers in the cell and the temperature of the cell block. Immediately after compression the pressure typically decreases by a factor of 2 in 5 s. In this region data are taken at a rate of six samples per second. After an hour it would take hours for such a pressure drop and the sampling time is lengthened to obtain more sensitivity.

The data are logged by a computer. Figure 5 shows the pressure and temperature measured during a typical de-

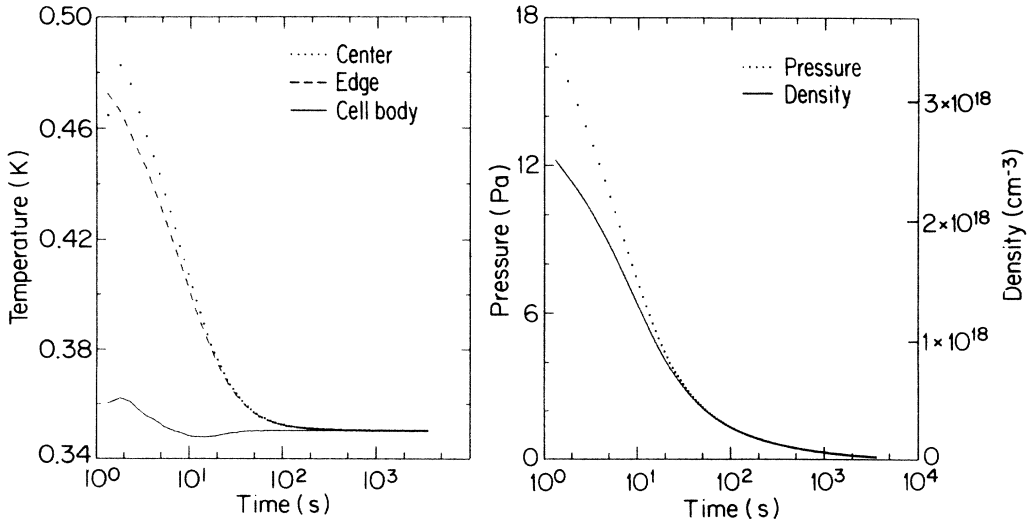


FIG. 5. Data taken during a decay at $B = 7.6$ T with a block temperature of 0.345 K. (a) Temperatures measured at the inner film thermometer (dashed line), the outer film thermometer (dotted line), and at the cell block (solid line). (b) Measured pressure (dotted line) and the computed density (solid line).

cay. The density computed from the data is also shown. The initial temperature rise is large and is rounded by the amplifier time constant. The subsequent agreement between the two film thermometers indicates that there is no horizontal temperature grandient in the gas between the center and the circumference of a sample cell. The cell block temperature, which is controlled, is also shown in the figure. The highest controlled density which we have observed was $4.5\times10^{18}$ atoms $cm^{-3}$. This occurred during a compression at a field of 7.6 T and a block temperature of 0.35 K. The gas temperature at that density had risen to 0.55 K.

It is not possible to burn off the hydrogen at the end of a run to find the baseline of the pressure transducer, as we did in earlier experiments,[6] since there is insufficient room in the cell for a recombination device. Lowering the piston is not helpful because of the large change in the pressure transducer frequency caused by stray capacitance (Sec. III C). Fortunately, because the pressure varies over two orders of magnitude or more, the known functional form of the low density behavior can be used to determine the baseline without having *a priori* information on the decay rates.

The baseline can be determined approximately by assuming a two-body decay behavior at long times, as expected at low density, which implies that the pressure varies inversely with time.[40] During final data processing, the density zero point is a free parameter in the fit to the decay equation, Eq. (56); its effect is small except at low temperatures. The quality of the fit provides a self consistent check. The uncertainty in the baseline due to the functional form chosen is certainly less than the final density, which itself is very small compared to the initial density.

At low densities during the first day or two of experimenting, the hydrogen decays exponentially with time. Presumably this is due to one-body relaxation of hydrogen interacting with magnetic impurities on the wall.[17,19] However, the one-body rate diminishes with each subsequent compression, and after the inside of the cell is coated with molecular hydrogen to a thickness of about 0.1 $\mu$m, the one-body rate becomes negligible. Thereafter, the decays are very reproducible.

The frequency of the pressure transducer oscillator varies linearly with the pressure in our pressure range; the film thermometers measure a temperature very close to that of the hydrogen gas (see Sec. V B). The ideal-gas equation is used to calculate the density $n$ as a function of time, for the densities are not high enough for quantum or non-ideal-gas corrections to be significant.

## V. DATA ANALYSIS

### A. Low-density, low-temperature determination of $G$ and $L$: the simple regime

At low density and $T<0.6$ K the simplified two- and three-body decay equation for H↓↑, Eq. (34), accurately describes of the system. Furthermore, it is in this regime that precise values of $G$ and $L$ are obtained. Equation (34) may be rewritten as

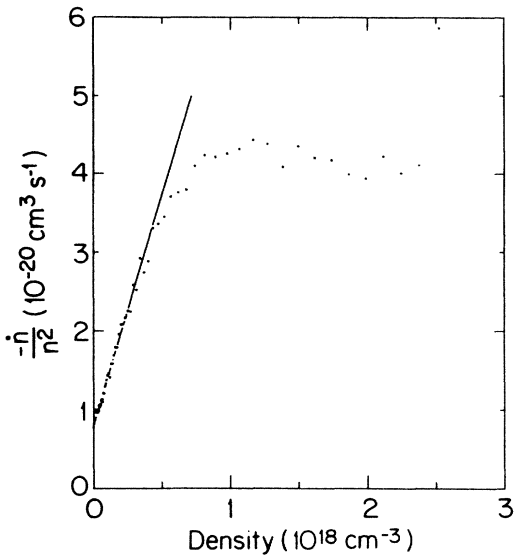


FIG. 6. $-\dot{n}/n^2$ for the decay shown in Fig. 5. The solid line is the best fit of the low-density part of the curve to Eq. (39). The slope of this line is $L$ and its intercept at $n=0$ is $2G$.

$$-\frac{1}{n^2}\frac{dn}{dt}=2G+Ln\ . \tag{39}$$

The most informative way to display the data is to plot $-(1/n^2)(dn/dt)$ as a function of $n$, as in Fig. 6. The intercept of the graph at $n=0$ gives twice the two-body relaxation rate $G$ and the slope gives the three-body recombination rate $L$. Decay due to one-body processes would be conspicuous on such a plot, for as explained below it would lead to a $1/n$ divergence at low $n$. Any variations of $G$ or $L$ during the decay, for instance due to changing temperature within the cell, would destroy the linearity of the plot. The data in Fig. 6 show that Eq. (39) accurately describes the data in the simple regime. Similar linear fits were used to determine $G$ and $L$ for all $T<0.6$.

### B. High-density or high-temperature regime

If $T\geq0.6$ K or if the heat generated by recombination significantly raises the temperature of part of the sample then the decay of the hydrogen density does not follow Eq. (39), and the system becomes far more complex. However, useful information on recombination, relaxation and transport properties is contained in data obtained in this regime. We analyzed the data by two models. The first is a "thermal model" that accurately accounts for effects caused by heating, but assumes that no relaxation occurs from the $c$ and $d$ states (see Appendix A). The second is a "four-state" model that includes all two body recombination processes, and many three-body recombination and two-body relaxation processes, but assumes a uniform and constant temperature.

*One-body decay.* One-body decay of spin-polarized hydrogen has been observed in earlier experiments[16,17,19] and appears in our results as well. It is presumably due to relaxation of the hydrogen adsorbed on the helium film induced by magnetic impurities in the solid cell walls.[17] In

our case the relaxation rate decreases with running time, due to the accumulation of a blanketing layer of $H_2$ between the walls and the helium film. A one-body surface relaxation rate $g_1$ can be taken into account by adding a term $2G_1/n$ to Eq. (39), where $G_1=g_1(A/V)(\sigma/n)$. The existence of such a term would be easily identifiable in the plots of $-(1/n^2)(dn/dt)$ because of its divergence at $n=0$.

*Incomplete nuclear polarization.* The steady-state nuclear polarization deviates from its ideal value of $-1$ depending on the operating conditions in the decaying gas. For temperatures above 0.50 K the deviation is sufficiently large to reduce the constant term in $-(1/n^2)(dn/dt)$ slightly below 2G [see Eq. (18)], and a correction must be made when analyzing the data. Furthermore, early in the decay the magnitude of the polarization can be smaller than the steady-state value, reflecting the conditions before the final compression step. As a result, at high density $-(1/n^2)(dn/dt)$ exceeds the value given by Eq. (39) as the excess $a$-state atoms decay by two-body and three-body recombination.

*Thermal effects.* The heat liberated by recombination causes a temperature gradient across the cell, altering the relative gas and surface densities. This gives rise to large changes in the pattern of the decay curves at high densities where the heating effects are largest.

In this section we examine these deviations from ideal behavior in order to understand quantitatively the approximations that are associated with Eq. (39) and to extract useful information about thermal transport in spin-polarized hydrogen experiments. The analysis is lengthy and quite detailed, but it should be borne in mind that the most important result of this study—the properties of three-body recombination coefficient $L$—are obtained almost entirely from the low-density data whose analysis is relatively simple and straightforward.

### 1. Density decay equations

Because of the possibility of temperature gradients in the compression chamber, the recombination must be examined separately for the gas and for the adsorbed layers on the lower and the upper surfaces. Five temperatures enter the calculations: the temperatures of the cell block, the hydrogen atoms on the lower $^4$He surface, the gas adjacent to the lower surface, the gas adjacent to the upper surface, and the hydrogen adsorbed on the upper $^4$He surface. These are indicated in Fig. 8.

During some compressions the surface density can become so high that the classical adsorption isotherm, Eq. (11), must be replaced by a more accurate theory. As the bulk density increases, $\sigma$ first rises over the classical value due to the quantum statistics of Bose particles, but then falls below it as the repulsive interaction causes the density to saturate.[41,42] Furthermore, because of the temperature gradients, a correction needs to be made for the small disequilibrium between the temperatures $T_s$ and $T_g$ of the surface and adjacent gas. It can be shown that

$$\sigma = r(T_g,T_s)\sigma_0 , \tag{40}$$

where $\sigma_0$ is the surface density in thermal equilibrium and $r$ is a correction factor given by

$$r=\frac{s(T_g)v(T_g)}{s(T_s)v(T_s)} . \tag{41}$$

Here $s$ is the sticking probability for an atom hitting the surface and $v$ is the mean speed. Zimmerman and Berlinsky[43] calculate that above 0.2 K, $s$ is roughly proportional to $T$, so that Eq. (41) becomes

$$r=(T_g/T_s)^{3/2} . \tag{42}$$

Incomplete nuclear polarization can significantly affect the decay. To account for this possibility, $\dot{n}_b$ and $\dot{n}_a$ must be computed separately. The coefficients of the three-body dipole terms for each species are the sum of two contributions. The first comes from the "prompt" recombination (Sec. II E). The same arguments in KVS that lead to Eq. (26) can be used to show that the decrease in the gas $b$-state density, for example, becomes

$$\dot{n}_b(\text{prompt}) = -C_g^d n_b(2n_b^2+\tfrac{4}{3}n_b n_a+\tfrac{2}{3}n_a^2) . \tag{43}$$

The second contribution comes from the "delayed" recombination of the single atom that is ejected from the three-body recombination collision, but with its electron spin flipped. Here we consider only the "thermal model" where $c$ and $d$ states immediately recombine.

$$\dot{n}_b(\text{delayed}) \approx -2N^d\frac{n_b}{n_b+n_a}C_g^d(n_b^3+n_b^2n_a+n_bn_a^2+n_a^3) , \tag{44}$$

where $N^d$ is the probability that the ejected atom is in the $c$ or $d$ state. We have used Eq. (16) with $K_o=K_p$ to show that the recombination rates with $a$ and $b$ partners are proportional to their respective densities. The factors in Eq. (44) have the following physical origin. If the ejected atom is in the $c$ or $d$ state, we assume it will recombine with a lower-state atom causing a net loss of two atoms. $n_b/(n_a+n_b)$ is an approximation to the probability that the atom which eventually recombines with the upper-state atom is in the $b$ state. The final factor is the probability of the initial three-body event.

The coefficients of the three-body exchange terms are simpler because no delayed recombination is associated with this process. Adding these three-body terms to the two-body relaxation terms, and neglecting flow to the surface, gives

$$\begin{aligned}
-\dot{n}_b &= G_g^{ba}(n_b^2-n_a^2)+G^{bc}(n_bn_a+2n_b^2)+G^{ad}n_an_b \\
&\quad + C_g^d n_b[(2+2N^d)n_b^2+\tfrac{4}{3}n_bn_a+(\tfrac{2}{3}+2N^d)n_a^2] \\
&\quad + C_g^{ex}(\tfrac{2}{9}n_bn_a^2-\tfrac{2}{3}n_a^3) , \\
-\dot{n}_a &= G_g^{ba}(n_a^2-n_b^2)+G^{ad}(n_an_b+2n_a^2)+G^{bc}n_an_b \\
&\quad + C_g^d n_a[(2+2N^d)n_a^2+\tfrac{4}{3}n_an_b+(\tfrac{2}{3}+2N^d)n_b^2] \\
&\quad + C_g^{ex}(\tfrac{8}{3}n_a^3+\tfrac{4}{9}n_a^2n_b) .
\end{aligned} \tag{45a}$$

The $c$ and $d$ state densities are not represented in our system of equations; therefore, electronic relaxation cannot be included in an exact fashion. We have introduced the

effects of electronic relaxation in the equations using a model based on two approximations. First, it is assumed that atoms which relax from $a$ or $b$ to $c$ or $d$ recombine before being able to return to either of the lower states. The $c$ or $d$ atom recombines on the wall, taking with it either an $a$ or $b$ atom with respective probability $n_a/n$ or $n_b/n$. The second approximation is that the electronic relaxation can be parametrized by a single relaxation rate constant $g^{bc}$ in terms of which all of the individual upward relaxation rates can be expressed as

$$\begin{aligned} G_{ab,ac} &= G_{bb,bc} = g^{bc} e^{-E_{bc}/k_B T} \equiv G^{bc} , \\ G_{ab,ad} &= G_{bb,bd} = 0 , \\ G_{ab,bd} &= G_{aa,ad} = g^{bc} e^{-E_{ad}/k_B T} \equiv G^{ad} , \\ G_{ab,bc} &= G_{aa,ac} = 0 . \end{aligned} \tag{45b}$$

Theoretical calculations of the individual electronic relaxation rate coefficients[22] indicate that the approximations of Eq. (45b) should be adequate for our purposes. Because the reaction rates in the gas are relatively insensitive to the temperature, these gas contributions to the decay are calculated assuming that the gas has a uniform temperature and density. Recall, also, that the KVS theory upon which these decay equations are based is strictly valid only at $T=0$. [This is discussed following Eq. (26).]

The three-body dipole recombination terms for the surface have the same structure as for the gas. Three-body exchange recombination, which is negligible compared to two-body surface recombination, is omitted, as is electronic relaxation on the surface. Again neglecting flow between the gas and the surface, one finds

$$\begin{aligned} -\dot{\sigma}_b &= (\sigma_b - \sigma_a) g_1 + K_{ab} \sigma_a \sigma_b + G_s (\sigma_b^2 - \sigma_a^2) \\ &\quad + C_s^d \sigma_b [(2+2N^d)\sigma_b^2 + \tfrac{4}{3}\sigma_b \sigma_a + (\tfrac{2}{3}+2N^d)\sigma_a^2] , \\ -\dot{\sigma}_a &= (\sigma_a - \sigma_b) g_1 + K_{ab} \sigma_a \sigma_b + 2K_{aa} \sigma_a^2 + G_s (\sigma_a^2 - \sigma_b^2) \\ &\quad + C_s^d \sigma_a [(2+2N^d)\sigma_a^2 + \tfrac{4}{3}\sigma_b \sigma_a + (\tfrac{2}{3}+2N^d)\sigma_b^2] . \end{aligned} \tag{46}$$

Flow across the gas-surface interfaces changes neither the total number of particles or the polarization of the system as a whole. The total time derivative of $N$ is thus

$$\frac{dN}{dt} = (\dot{n}_a + \dot{n}_b) V + (\dot{\sigma}_{l,a} + \dot{\sigma}_{l,b} + \dot{\sigma}_{u,a} + \dot{\sigma}_{u,b}) A \tag{47}$$

where $u$ stands for the upper surface and $l$ the lower surface. The total derivative of the gas density is

$$\frac{dn}{dt} = \frac{dN}{dt} \frac{n}{nV + \sigma_u A + \sigma_l A} . \tag{48}$$

This quantity can be determined from the pressure and temperature data, allowing the model to be compared with experiments.

### 2. *Thermal resistances*

This discussion pertains only to the "thermal model," and consequently we shall assume that the $c$ and $d$ states instantly recombine. Three resistances contribute to the temperature difference between the copper base of the compression cell and the thermometer on the Kapton diaphragm on the upper surface of the pancake cell: the Kapitza boundary resistance between the copper and the helium film, a boundary resistance between the helium film and the gas, and the thermal conductivity of the gas.

The Kapitza resistance $R_K$, which increases rapidly with decreasing temperature, is the dominant thermal resistance at low temperatures. The solid line in Fig. 7 shows measured values of $R_K$ for an interface between polished copper and liquid $^4$He.[44] The silver powder sintered to the surface of the copper in our cell increases its surface area, and the effective value of $R_K$ is expected to be significantly smaller than the value for a polished surface. The actual values of $R_K$, determined from a fit to the complete thermal model as discussed below, are shown in Fig. 7. The sinter decreases the resistance by a factor of $\sim 4$.

The temperature difference between the helium film and the copper block is

$$\Delta T = \frac{R_K \dot{Q}}{A} , \tag{49}$$

where $\dot{Q}$ is the heat flux and $A$ is the area. This expression assumes that $\Delta T$ varies linearly with $\dot{Q}$, which may not be true at the beginning of a decay when $\Delta T \sim T$.

The boundary resistance between the gas and the helium surface can be parametrized by a simple kinetic model. Let $T$ be the temperature of the helium film and $T+\Delta T$ be the temperature of the gas adjacent to the film. If one assumes that on the average a fraction $\alpha$ of a gas

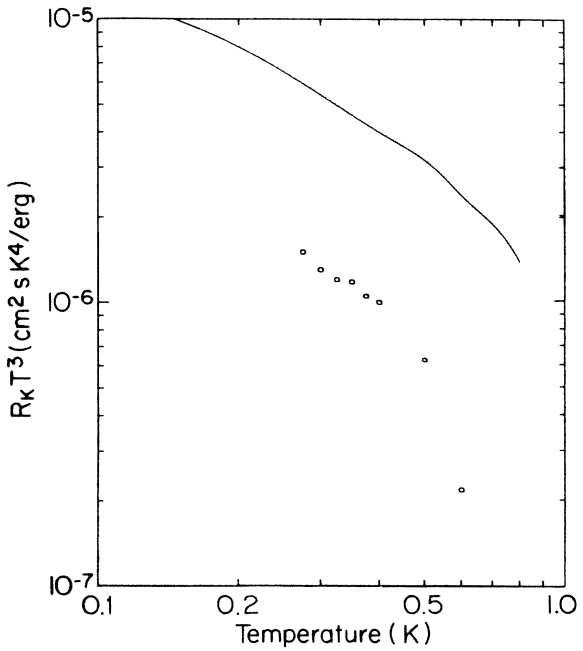


FIG. 7. Liquid-solid Kapitza resistance $R_K$. The solid line indicates the experimental values of $R_K$ between liquid $^4$He and polished copper measured by Anderson *et al.* (Ref. 44). The circle indicate the effective values of $R_K$ for the sintered silver on copper in our cell as determined by the temperature rise during a decay.

atom's excess kinetic energy is transferred to the film during a collision, then the associated gas-liquid boundary resistance, $R_{gl}$, is

$$R_{gl}=(\tfrac{1}{2}\alpha n k_B\langle v\rangle)^{-1}\ , \tag{50}$$

where $\langle v\rangle=(8k_BT/\pi m)^{1/2}$ is the mean thermal speed in the gas. The fraction $\alpha$, the accommodation coefficient,[45] cannot be smaller than the probability $s$ that an incoming hydrogen atom sticks to the surface. Jochemsen *et al.*[46] used the wall shift of the hyperfine resonance to determine that $s=0.035(4)$ near $T=0.2$ K. Previous experiments on $H_\downarrow$ have yielded values of $\alpha$ in the range 0.20 to 0.35.[47,48] The value of $\alpha$ in our experiments ranges from 0.8 at 0.6 K to about 0.4 at 0.3 K. $R_{gl}$, which is inversely proportional to $n$, becomes the dominant thermal resistance at low densities. Theoretical calculations of $R_{gl}$ are now available,[49–51] and it is to be hoped that precise measurements will be carried out in the near future.

The thermal conductivity $\kappa$ of $H\downarrow\uparrow$ has been calculated by Lhuillier.[52] Between 0.1 and 1.0 K she finds that $\kappa$ is approximately 360 erg $K^{-1}s^{-1}$. The temperature rise across the gas depends on where the heat originates. If the heat enters the gas at the top of the cell, the temperature difference between the bottom and the top is obtained from an effective thermal resistance

$$R_g=\frac{w}{\kappa}\ , \tag{51}$$

where $w$ is the separation between the two flat walls of the compression chamber. If, on the other hand, the heat is deposited uniformly throughout the gas (or in any other fashion symmetric about the midplane) the effective thermal resistance becomes

$$R_g=\tfrac{1}{2}\frac{w}{\kappa}\ . \tag{52}$$

This contribution to the thermal resistance of the cell is roughly constant throughout our measurements. It is the dominant contribution at high temperatures.

A treatment of temperature rises in the gas under the more extreme conditions leading to explosive recombination has been given by Kagan *et al.*[39]

### 3. *Distribution of heat*

It is convenient to define several heat fluxes associated with the recombining hydrogen. Let $j_g$ be the heat flux arising from recombination in the gas and $j_u$ and $j_l$ be the fluxes from recombination in the upper and lower adsorbed layers of hydrogen. The only type of recombination taking place in the gas is the prompt recombination during a three-body collision. The corresponding heat flux is

$$j_g=\frac{D_0}{2}w(2W_g^d+2W_g^{ex})n\ , \tag{53}$$

where $D_0$ is the energy released when two atoms recombine, and $W_g^{ex}$ and $W_g^d$ are given by Eqs. (25) and (26). Another contribution to the heat flux is from the delayed recombination that occurs after a three-body event takes place on the helium film. This heat is divided between the two surfaces in proportion to the surface densities. When added to the heat from the other sources of recombination on the surface, this leads to the equations

$$\begin{aligned} j_u&=D_0\left[\frac{\sigma_u}{\sigma_l+\sigma_u}wN^dW_g^dn+\dot\sigma_u\right]\ ,\\ j_l&=D_0\left[\frac{\sigma_l}{\sigma_u+\sigma_l}wN^dW_g^dn+\dot\sigma_l\right]\ . \end{aligned} \tag{54}$$

These $j$'s in Eqs. (53) and (54) refer to where the $H_2$ molecules are formed, not where the heat of recombination is deposited. We will assume that the heat associated with $j_g$ is deposited uniformly throughout the gas. Molecules forming on the surface acquire large kinetic energy and will either fly into the gas or bury themselves in the helium film. To take this into account, we define $F$ to be the fraction of the recombination energy of the molecules formed on a surface which is deposited directly into the helium film. We know of no measurements or theoretical estimates for $F$. Fortunately, the experimental results are not very sensitive to its value, as will be seen below.

Finally, we must model how the remaining fraction, $1-F$, of the surface recombination energy is distributed in the gas. In the density range from $10^{17}$ to $10^{18}$ atoms $cm^{-3}$ the width of the cell is between 2 and 20 mean free paths. The mean free path for highly excited $H_2$ in the H gas may be somewhat shorter, but probably not by an order of magnitude. It is expected that many collisions are required for $H_2$ to relax from its highest vibrational state ($v=14$) to the ground state. Therefore, in most of the analysis we make the simplest assumption that this recombination energy is distributed uniformly throughout the gas. If we take the other extreme and assume that the heat from a surface is deposited just outside in the gas, the numerical results for $\dot n$ and the total $\Delta T$ are little affected, as shown below.

The temperatures at various locations in the cell can be determined from these assumptions using the electrical circuit analogy shown in Fig. 8. Only the total temperature difference across the cell, $T_m-T_s$, can be measured, but the other temperatures are necessary to specify the surface densities used to calculate the decay.

To analyze the decay curves in the high-density regime, Eqs. (45) and (46) for $\dot n$ and $\dot\sigma$ and the temperature distribution from Fig. 8 were solved iteratively at each density until self-consistency was achieved. The resulting values of $\dot n_a$ and $\dot n_b$ were then used to determine the densities at the next time increment.

Computer solutions for these equations show that the decays are relatively insensitive to the value of $F$. This can be understood from Fig. 8 as follows. If the upper and lower surface densities differ by only a small percentage, as is the case when the temperature difference across the cell is small, the currents $j_u$ and $j_l$ are quite close in value. Suppose that $j_u=j_0-\delta$ and $j_l=j_0+\delta$; then

$$\begin{aligned} T_m-T_s&=\tfrac{1}{2}(j_g+2j_0-2\delta)R_g\\ &\quad+(j_g+2j_0-2\delta F)R_{gl}+(j_g+2j_0)R_K\\ &\approx(j_g+2j_0)(R_K+R_{gl}+\tfrac{1}{2}R_g)\ . \end{aligned} \tag{55}$$

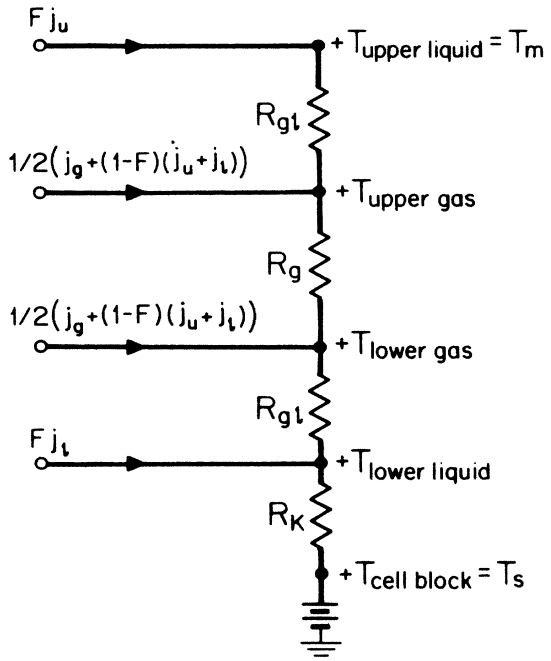


FIG. 8. Electrical analogy for the model of heat distribution in the sample chamber. The temperatures correspond to voltages and the recombination heats $j$ correspond to currents.

To lowest order, the temperature gradient depends neither on $F$ nor on how the heat is distributed in the gas.

#### 4. *Modeling the data*

The experiments measure the density of the gaseous spin-polarized hydrogen $n(t)$ and the temperature rise across the cell $\Delta T(t)=T_m-T_s$ as functions of time during a decay. The density measurements are displayed in the form $-\dot{n}/n^2$ versus $n$ in order to facilitate the identification of one-, two-, and three-body processes. The temperature measurements are displayed as $-\Delta T/\dot{n}$ versus $n$ since this quantity is proportional to the various thermal resistances. (The Kapitza resistance and gaseous conductivity are independent of $n$; the gas-liquid interface resistance varies as $1/n$).

Figures 9—11 show representative results at cell block temperatures of 0.600, 0.375, and 0.300 K. Also shown in the figures are simulated decays based on numerical solutions of the "thermal model." With the exception of $W_g^{ex}$, the values of the various rate constants are chosen to give the best fits to the decays at low densities. In this limit the experimental results can always be fit to within the noise. The discussion which follows centers on our ability to reproduce the results at the high-density region of each trace.

The data in Fig. 9 were taken at 0.600 K, the highest temperature at which we could work at high densities without encountering serious problems due to thermal explosions.[9,38,39] Figure 9(a) shows that at densities above $1\times10^{18}$ cm$^{-3}$, $-\dot{n}/n^2$ varies more rapidly than the linear dependence on $n$ indicated by Eq. (39). Such behavior is predicted by the model when the magnitude of the initial nuclear polarization of the gas, $P_n=(n_a-n_b)/(n_a+n_b)$, is chosen to be lower than its steady-state value at this temperature, $-0.907$. However, in order to obtain a quantitative fit, both at this temperature and at 0.5 K, the three-body exchange recombination involving *aab* [see Eq. (28)] must be included. We are able to fit each trace to within the noise by choosing appropriate values of $C_g^{ex}$ and the initial polarization. Figure 9(a) demonstrates the sensitivity of the fits to these parameters. We find $C_g^{ex}=3.5(15)\times10^{-36}$ cm$^6$s$^{-1}$ at $B=7.6$ T. The calculations of KVS lead to the value $C_g^{ex}\approx3\times10^{-37}$ cm$^6$s$^{-1}$ at this magnetic field. At a temperature of 0.6 K, the measured value of $C_g^{ex}$ increases rapidly with decreasing mag-

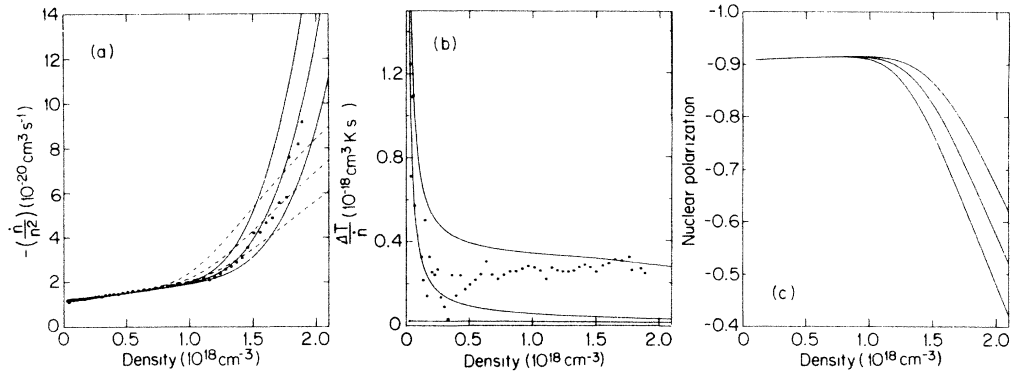


FIG. 9. Experimental data and model results at $T=0.600$ K and $B=7.6$ T. (a) $-\dot{n}/n^2$. The dashed curves show model results assuming $C_g^{ex}=0$ for three different initial nuclear polarizations: $-0.55$ (upper curve), $-0.65$, and $-0.75$. The solid lines show model results for $C_g^{ex}=3.5(15)\times10^{-36}$ cm$^6$s$^{-1}$ and the same three initial polarizations. (b) The thermal resistances during the decay. The solid lines indicate, beginning with the lowest, the resistance from the cell block to liquid on the bottom surface, from the cell block to the lowest part of the gas, and from the cell block to the top of the gas. It is the highest of these curves, the total thermal resistance across the cell, which should be compared to the data. (c) The time evolution of the nuclear polarization as predicted by the model for the three different initial values.

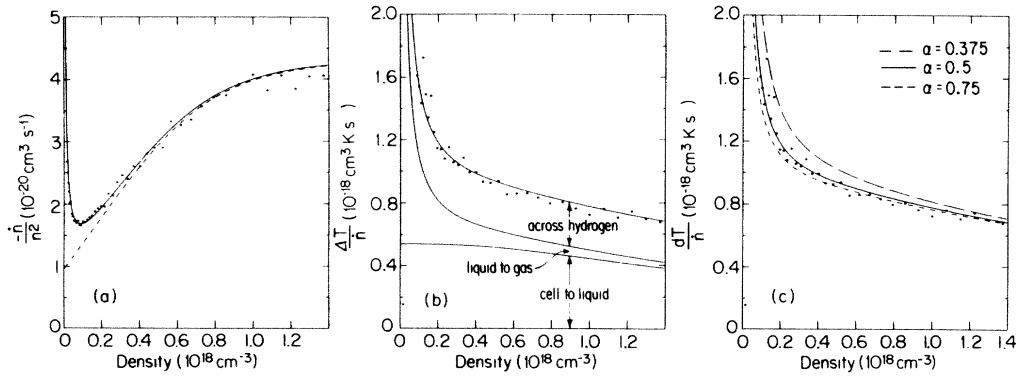


FIG. 10. Experimental data and model results at $T=0.375$ K and $B=7.6$ T. (a) $-\dot{n}/n^2$. This decay shows the presence of one-body relaxation, as indicated by the upturn in the data at low densities. The roll-over in the decay data at high densities is due to heating effects. The solid line is a fit including the one-body rate; the dashed line is the result obtained if the one-body rate is set to zero while the other parameters are kept the same. (b) The thermal resistances. The difference between the lower and middle solid curves is due to the gas-liquid resistance, which depends on the accommodation coefficient $\alpha$. (c) The effect on the total resistance caused by changing $\alpha$ from 0.75 (dashed line) to 0.5 (solid line) and to 0.375 (dot-dashed line).

netic field between 4 and 8 T; the form of the field dependence is consistent with that calculated theoretically.[8]

It is just these conditions—relatively high temperatures and only modest polarization—under which the temperature dependent *abb* contributions to the exchange recombination can be important (see Sec. II E). We have tried to fit traces similar to Fig. 9(a) taken at 0.6 and 0.5 K by setting $C_g^{ex}=0$ and using instead a three-body exchange process of the form $\dot{n}=-2C^{abb}n_a n_b^2$. The resulting fits to individual traces, although plausible, were not as convincing as those obtained using $C_g^{ex}$ with $C^{abb}=0$. In particular the transition from high $\dot{n}/n^2$ early in a decay to modest $\dot{n}/n^2$ later occurred too abruptly when using the *abb* process. The best fits for *abb* recombination were obtained with $C^{abb}=3\times10^{-37}$ cm$^6$s$^{-1}$. However, this is about 300 times the value one would estimate from the work of Greben, Thomas, and Berlinsky.[21] We conclude, therefore, both from the quality of the fits and from the proximity of the measured and estimated coefficients, that the rapid decay rates early in the high-temperature traces are caused by the three-body exchange process discussed by KVS and represented by $C_g^{ex}$.

Figure 9(c) shows how the polarization approaches its steady-state value; in the steady-state regime, $-\dot{n}/n^2$ data can be represented by the linear behavior of Eq. (39). However, the intercept at $n=0$ in Fig. 9(a) is at $1.09\times10^{-20}$ whereas $2G=1.25\times10^{-20}$ cm$^3$s$^{-1}$. This 13% decrease is caused by incomplete steady-state polarization.

The data for $-\Delta T/\dot{n}$ are displayed with the thermal model curve in Fig. 9(b). For comparison, the various contributions to the model curve are also displayed: the temperature rise from the cell to the liquid helium on the lower surface due to the Kapitza resistance, to the gas just

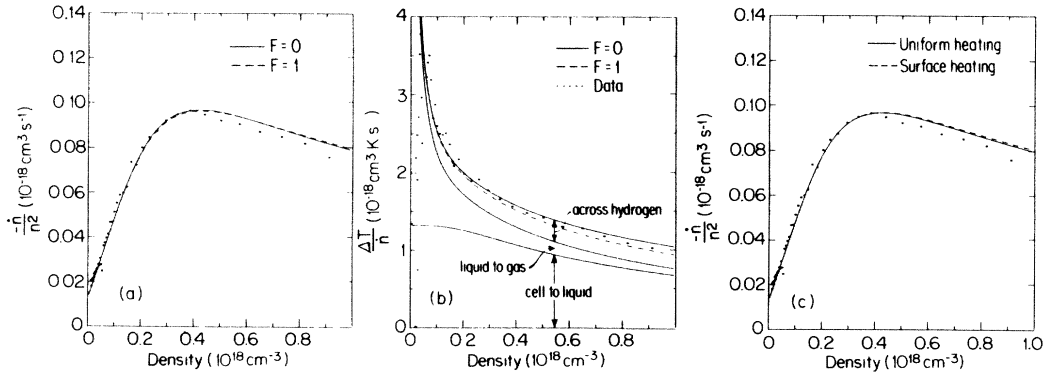


FIG. 11. Experimental data and model results at 0.300 K and 7.6 T. (a) $-\dot{n}/n^2$. The model calculation shows that whether the surface recombination heat is deposited locally in the helium film (dashed line) or whether it is distributed throughout the gaseous $H_1$ (solid line) has little effect on the overall decay of the sample. The thermal resistance calculations in (b) show that the above two alternatives cause different temperatures for the gas just above the lower surface, but do not change the temperature of the liquid on that surface and have little effect on the total temperature rise across the cell. In (c) we show that if the surface recombination heat is deposited in the gas, its distribution has negligible effect on the decay. The solid curve assumes uniform heating of the gas; the dashed curve is for heating localized next to the surfaces.

above the lower surface due to the Kapitza resistance and the accommodation coefficient, and the temperature of the upper measured surface. In all these fits the thermal conductivity of the gas was fixed at the theoretical value.[52] In the Fig. 9(b) this accounts for almost all of the temperature rise. At this temperature the best fit to the data was achieved with an accommodation coefficient $\alpha \approx 0.8$, although the fit is only sensative to $\alpha$ at low density where the noise in the data is relatively high.

The data in Fig. 10 were taken at 0.375 K. At this temperature the decay equations show that the hydrogen becomes completely polarized so rapidly that the nuclear polarization can be assumed to be nearly $-1.0$ for all densities displayed. The low-density region of $-\dot{n}/n^2$ shows a clear contribution from a one-body process $g_1$. The solid line is a fit taking this process into account, and the dashed line is generated using the same parameters, except with $g_1=0$. (This trace was chosen specifically to display the effect of a one-body process; most of the data at this temperature showed a negligible contribution from $g_1$.) At higher densities $-\dot{n}/n^2$ falls below the linear behavior of Eq. (39) since the surface density (and therefore the surface contribution to $L$) is decreased due to the temperature gradient in the cell. The model reproduces this behavior to within the noise.

The temperature rise data in Fig. 10(b) clearly shows the effect of the accommodation coefficient on the results at low density. The Kapitza resistance now accounts for about half of the temperature rise at modest densities. Figure 10(c) shows the effect of varying the accommodation coefficient while holding the Kapitza resistance and gas conductivity constant.

The data in Fig. 11 were taken at a cell temperature of 0.300 K. When the hydrogen reaches that temperature, 97% of $L$ is due to the surface contribution. The model describes the thermal effects on $-\dot{n}/n^2$ quite well; the small difference at the highest density may be due to the nonideal geometry of the cell. At this temperature a model simulation was done for the limiting cases of $F=1$ (surface recombination heat is deposited entirely in the helium film) and $F=0$ (surface recombination heat is deposited entirely in the gas). The effect on $-\dot{n}/n^2$ is negligible. The effect on $-\Delta T/\dot{n}$ is larger, about 10% at the highest density, but this is small compared to the other uncertainties involved in extracting thermal parameters from the data.

In Fig. 11(c) we show the effect of changing the way the heat from recombination on the surface is distributed in the gas: in one case the heat from the surface that does not go into the liquid is assumed to uniformly heat the gas, in the other case it is assumed to be deposited in the gas next to the surface of origin. The change in $-\dot{n}/n^2$ is again negligible.

We have carried out model fits to the data, with one or both of our models, for all the temperatures at which we made measurements. In addition, we have done least-squares fits of the low-density part of each decay below 0.6 K to the form

$$-\dot{n}=G_1(n-z)+2G(n-z)^2+L(n-z)^3 \tag{56}$$

to obtain the effective one-body rate $G_1$, the effective two-body coefficient $G$, the three-body rate coefficient $L$, and the density zero $z$. The model fits show that the least-squares fit results for $G_1$ and $L$ are correct for $T<0.6$ K, except for a very small adjustment to account for incomplete nuclear polarization. Under these conditions, $G \approx G^{bc}+G^{ab}$ [see Eq. (35)] and $L \approx C^d(2+2N^d)$ within 5% [see Eq. (32)]. The thermal effects are adequately explained by the theoretical gas conductivity,[51] an effective Kapitza resistance given by the values in Fig. 7, and an accommodation coefficient which varies from near 0.8(4) at 0.60 K to about 0.4(2) at 0.275 K.

### 5. *Four-state model*

The major portion of our data was modeled without calculating the individual behavior of the upper hyperfine states, $c$ and $d$, as described above. However, for $T>0.6$ K we calculated their evolution separately. The rationale for this model is that at high temperatures $c$ and $d$ atoms can relax back to the lower two states before they recombine, contrary to the assumptions of the thermal model. We did not follow variations in the sample temperature as this model was intended for use at $T \geq 0.6$ K where the results should be relatively insensitive to temperature fluctuations.

The four-state model assumes that $n_c+n_d \ll n_a+n_b$, self-heating is small, the rates for all processes involving two upper-state atoms are small compared to rates involving collisions of upper- and lower-state atoms, and that the time for $n_c$ and $n_d$ to reach equilibrium is small compared to $n/\dot{n}$. All of these assumptions are verified internally by the program, with the exception of the self-heating requirement. The assumptions of small $c$- and $d$-state densities and short equilibrium times for $c$ and $d$ atoms allow the equations to be simplified by expressing $n_c=n_c(n_a,n_b)$, and $n_d=n_d(n_a,n_b)$ thus reducing a stiff four-variable differential equation to a two-variable numerically tractable case. Typical time scales for the upper-state atoms to reach equilibrium density are on the order of $\tau_{eq}=(G^{bc}n_b)^{-1}=10^{-3}$s at $n=10^{18}$ cm$^{-3}$ or 1 s at $n=10^{15}$ cm$^{-3}$. The characteristic time for the total number density to change at corresponding densities are $>1$ s and $>10^3$ s, respectively.

The following rate constants were included in the simulations.

(i) $K_{\alpha\beta}$ with $\alpha$, $\beta$ in the set of $\{a,b,c,d,\}$ as defined by Eq. (16).

(ii) The following relaxation processes: $a+b \leftrightarrow a+a$, $b+b \leftrightarrow a+b$, $c+c \leftrightarrow b+d$, $b+d \leftrightarrow a+a$, $a+c \leftrightarrow a+a$, $c+d \leftrightarrow a+b$, $d+d \leftrightarrow a+a$, $b+d \leftrightarrow a+b$, $c+d \leftrightarrow b+d$, $c+d \leftrightarrow a+c$, $a+c \leftrightarrow a+b$, $b+d \leftrightarrow a+c$, $c+c \leftrightarrow b+b$, $b+c \leftrightarrow b+b$, $d+d \leftrightarrow a+d$, $a+d \leftrightarrow a+a$, and $c+c \leftrightarrow b+c$ from Lagendijk *et al.*[22]

(iii) The three-body processes in Table I. All relaxation rates were included that could be expected to affect densities at the $10^{-3}$ level.

The set of parameters which were used in the fits were $K_o$, $K_p$, $C^d$, $C^{ex}$, $C^{ul}/C^{ex}$, $G^{bc}$, and the initial conditions (density, polarization, and zero offset). $K_o$ and $K_p$ were set from $K_s$ and $\gamma$ above Eq. (16), then used in Eq. (16), and $G^{bc}$ was used to set

TABLE I. Three-body processes included in the four-state model. The columns are the incoming hydrogen atoms for each process, the parameterization of the rate constant for the fits, and the hypothesized probability distribution of the products. Note that $a+a+a$ and $a+a+b$ are included twice: they can react via either the dipole-dipole or exchange mechanisms.

| Reactants | Rate constant | Product fractions | | | | |
|---|---|---|---|---|---|---|
| $a+a+a$ | $C^d$ | $a$:0.07 | | | $d$:0.93 | $+H_2$ |
| $a+a+a$ | $C^{ex}$ | $a:\frac{1}{3}$ | $b:\frac{2}{3}$ | | | $+H_2$ |
| $a+a+b$ | $C^d$ | $a$:0.07 | $b$:0.047 | $c$:0.31 | $d$:0.62 | $+H_2$ |
| $a+a+b$ | $C^{ex}$ | $a:\frac{2}{3}$ | $b:\frac{1}{3}$ | | | $+H_2$ |
| $a+b+b$ | $C^d$ | $a$:0.023 | $b$:0.047 | $c$:0.62 | $d$:0.31 | $+H_2$ |
| $b+b+b$ | $C^d$ | | $b$:0.07 | $c$:0.93 | | $+H_2$ |
| $a+a+c$ | $C^{ul}$ | $a$:1 | | | | $+H_2$ |
| $a+b+c$ | $C^{ul}$ | $a:\frac{1}{2}$ | $b:\frac{1}{2}$ | | | $+H_2$ |
| $b+b+c$ | $C^{ul}$ | | $b$:1 | | | $+H_2$ |
| $a+a+d$ | $C^{ul}$ | $a$:1 | | | | $+H_2$ |
| $a+b+d$ | $C^{ul}$ | $a:\frac{1}{2}$ | $b:\frac{1}{2}$ | | | $+H_2$ |
| $b+b+d$ | $C^{ul}$ | | $b$:1 | | | $+H_2$ |

$$G_{bc,bb}=G_{dd,ad}=G_{ad,aa}=G_{cc,bc}=G^{bc}\ .$$

$C^{ul}/C^{ex}$ was set to $10/\sin^2\theta$ or $1/\sin^2\theta$ without affecting results, and a $\sin^2\theta$ field dependence was assumed for $C^{ex}$. A robust nonlinear fitting program based on algorithms by Huber,[53] Marquardt,[54] and Broyden[55] was used to fit $n(t)$ to the model.

We were able to determine $C^d$ and $G^{bc}$ accurately, $C^{ex}$ for some traces, $K_p$ poorly, and our fits were not sensitive to $C^{ul}$ or $K_o$. The important three-body parameter combination seemed to be approximately $(1+N^d)C^d$, so if $N^d$ varied from our assumed 0.93, $C^d$ would be affected. The main problem with $C^{ex}$ was sensitivity to $K_o$ and $K_p$; these fits gave values of $C^{ex}$ which were in agreement with those obtained from the thermal model.

## VI. RESULTS

Extensive measurements on relaxation and recombination were carried out at various temperatures and magnetic fields. Most of the data were taken using surfaces coated with $^4$He, but measurements were also made using mixtures of $^3$He and $^4$He. In this section the experimental results are presented and interpreted in terms of the underlying physical processes. Because every process has its own characteristic temperature and field dependence, the most accurate parameters are obtained by fitting both the $T$ and $B$ dependences of the data simultaneously. Fits were done by the procedure described in Sec. V B 5 for $T\geq 0.6$ K and the procedure of Sec. V A for $T<0.6$ K. The numerical results are summarized in Table II. Appendix D contains a glossary of the symbols.

### A. Two-body relaxation processes

Figure 12 displays our data for the two-body relaxation constant $G$ as a function of magnetic field and inverse temperature. The surface represents a three-parameter fit based on

$$G(B,T)=\phi G_g^{ba}(B,T)+G_s^{ba}(B,T)\frac{A}{V}\Lambda^2(T)e^{-2E_b/k_BT}+g^{bc}e^{-2\mu B/k_BT}\ . \tag{57}$$

The first two terms describe $b\rightarrow a$ transitions due to

TABLE II. A summary of numerical values obtained in these experiments. Symbols are defined in the glossary, Appendix D.

| Parameter | Value | Notes |
|---|---|---|
| $\Gamma_s^{ba}$ | less than $2\times10^{-14}$ cm$^2$s$^{-1}$ | |
| $g^{bc}$ | $1.03(9)\times10^{-15}$ cm$^3$s$^{-1}$ | This is a volume rate, as the data were only sensitive to $g^{bc}$ at higher temperatures. |
| $\varphi$ | 1.06(4) | Ratio of observed $G_v^{ba}$ to $G_v^{ba}$ derived from Eq. (20) |
| $L_s$ | $8.9(8)\times10^{-39}$ cm$^4$s$^{-1}$ | At 7.6 T |
| $L_g$ | $1.2(4)\times10^{-24}$ cm$^6$s$^{-1}$ | At 7.6 T |
| $E_b$ | 1.04(3) | From fit for $L_s$ and $L_g$ |
| $\zeta$ | $-0.07(2)$ T$^{-1}$ | Assuming $\zeta_g\approx\zeta_s$ |

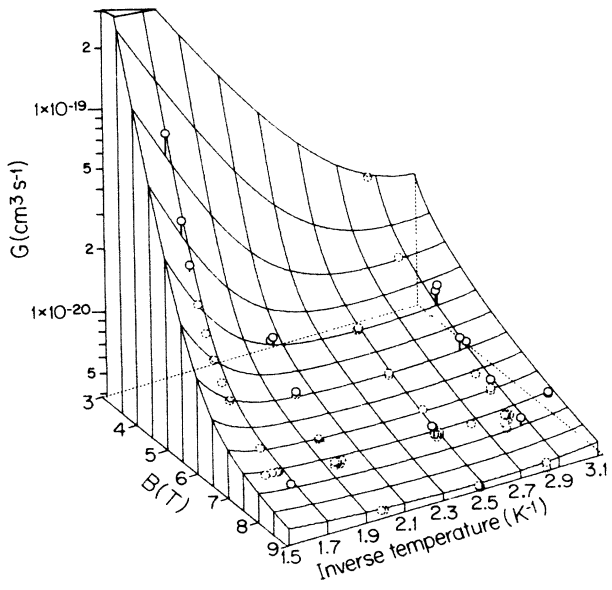


FIG. 12. Temperature and magnetic field dependence of the relaxation rate $G$. The spheres are our measurements, and the plotted surface is our fit to Eq. (57). Solid circles are completely above the surface, dashed circles intersect the fitted surface, and dotted circles are completely below the surface.

volume and surface nuclear relaxation, respectively, while the last term accounts for $b \rightarrow c$ transitions in the gas due to electronic relaxation. This representation of $G$ as made up of additive components is valid so long as any transition out of the $b$ state results in a recombination. To the accuracy of our measurements, this is the case below 0.6 K. We discuss each of these in turn. In this section, the value for binding energy $E_b$ was taken to be 1.04(3) K, as discussed in Sec. VI B, below.

### 1. Volume nuclear relaxation

We have chosen to express our results for $G_g^{ba}$ in terms of the theoretical value calculated by van der Eijnde,[23] Eq. (20). The fitting parameter $\phi$ was determined to be 1.06(4). This represents experimental confirmation of Eq. (20) in the $B-T$ region studied.

### 2. Surface nuclear relaxation

$G_s^{ba}$ was parametrized as $\Gamma_s^{ba}F(B)$, where $F(B)$ represents the field dependence of the effective magnetic moment, Eq. (20b), and $\Gamma_s^{ba}$ is the remainder of the two-body surface relaxation rate. Our data were capable only of placing an upper limit on the surface relaxation rate constant: $\Gamma_s^{ba} < 2\times10^{-14}$ cm$^{-2}$ s$^{-1}$.

Because the surface density increases rapidly, as the temperature is decreased, three-body processes overshadow both surface and bulk two-body processes. Consequently, no useful information on $G$ could be extracted below 0.325 K, although data on the three-body recombination rate $L$ were obtained down to 0.250 K. Our upper limit on $G_s^{ba}$ is consistent with recent ESR measurements by Reynolds *et al.*[56] Both of these results indicate that $G_s^{ba}$ is much smaller than earlier reported experimental values,[6,16,10] which were in the vicinity of $9\times10^{-14}F(B)$ cm$^2$s$^{-1}$. We now believe that all of these earlier results were in error. As explained in Appendix B, the then-unrecognized three-body recombination processes were misinterpreted as a two-body surface rate.

### 3. Electronic relaxation in the gas

We obtain $g^{bc}=1.03(7)\times10^{-15}$ cm$^{-3}$s$^{-1}$ both from Eq. (57) and directly from the four-state model. Our result in the vicinity of $T=0.55$ K is in good agreement with the value of $8(4)\times10^{-16}$ cm$^3$s$^{-1}$ measured by Sprik *et al.*[9] at 0.710 K, or the recent reanalysis of their data,[57] which gives $1.2(4)\times10^{-15}$ cm$^3$s$-1$. KVS (Ref. 8) estimate $g^{bc}$ to be on the order of $2\times10^{-15}$ cm$^3$s$^{-1}$, and a recent detailed calculation by Lagendijk, van Yperen, and Walraven[58] gives $9.17\times10^{-16}$ cm$^3$s$^{-1}$. Thus our results for electronic relaxation are consistent with theoretical calculations, and are more accurate than previous experimental results.

### 4. Qualitative features of the G(B,T) surface

The general topography of the surface in Fig. 12 can be understood in terms of the underlying processes. The gentle rise of $G$ at low temperatures as one proceeds toward low fields is due to the increase of the effective nuclear moment of the $a$ state. This is accounted for by the factor $F(B)$ in $G_s^{ba}$ and in Eq. (20). The stronger increase in $G$ at the high-temperature, low-field corner of the plot is due to collisions which flip the electron spin between the $b$ and $c$ states. Because energy $E_{bc}$ is required to reverse the electron spin, this process is surpressed by the Boltzmann factor of $\exp(-E_{bc}/k_BT)$. The role of electron spin relaxation can be seen with greater clarity in Fig. 13 which displays constant temperature slices of the data at 0.35 and 0.6 K. The solid curves are the complete

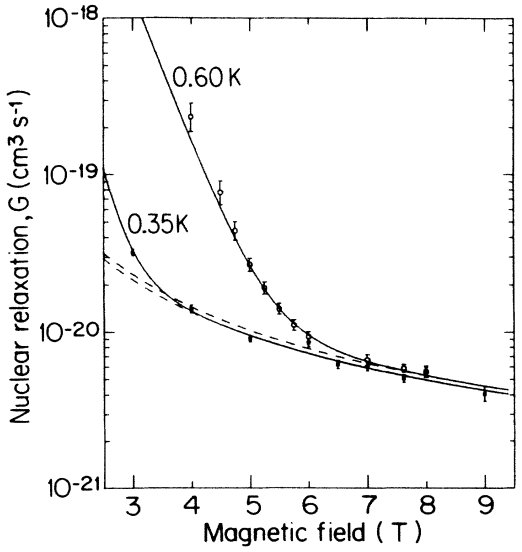


FIG. 13. Magnetic field dependence of the relaxation rate constant $G$. Circles are results at $T=0.60$ K, solid squares at $T=0.35$ K. Our fit to the data [Eq. (57)] is given by the solid lines, and the dashed lines show the effect of eliminating $g^{bc}$.

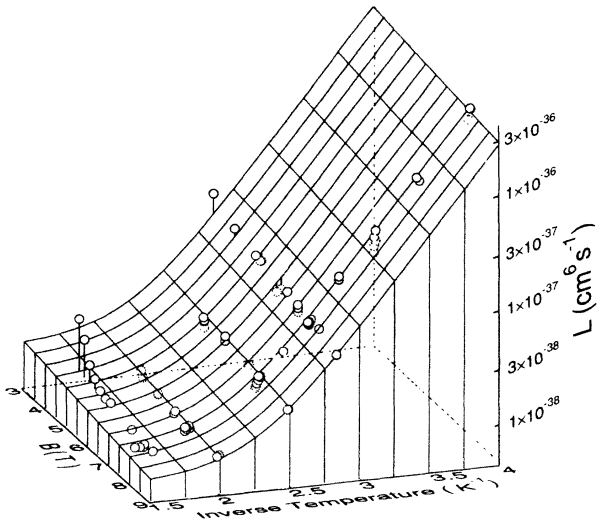


FIG. 14. Temperature and magnetic field dependence of the three-body recombination rate $L$. The spheres are our measurements, and the plotted surface is our fit to Eq. (58). Solid circle are completely above the surface, dashed circles intersect the fitted surface, and dotted circles are completely below the surface.

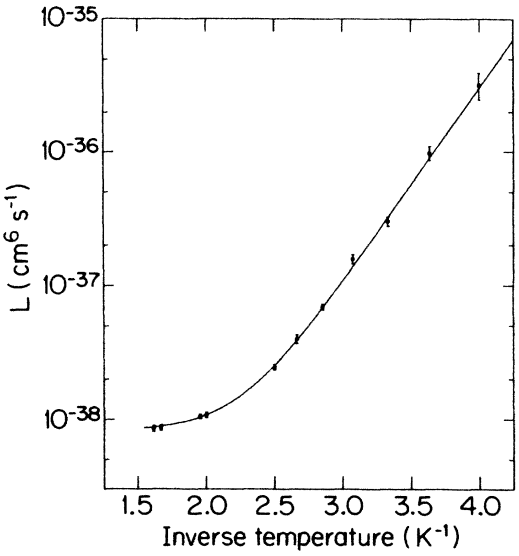


FIG. 15. Temperature dependence of the three-body recombination rate constant $L$ at $B=7.62$ T. The solid line is our fit to Eq. (58).

fit, while the dashed curves display the same expression with $g^{bc}$ set to zero.

### B. Three-body recombination processes

Figure 14 displays our data for the three-body recombination rate constant $L$ as a function of temperature and magnetic field. The high-field and high-temperature corner is dominated by a gas-phase process; the low-temperature edge is controlled by surface three-body recombination. We believe that the small rise at $T=0.6$ K for $B \leq 5$ T is a systematic error due to neglect of the self-heating of the gas by the "four-state model." A slice of the surface at $B=7.62$ T is shown in Fig. 15. The high signal-to-noise ratio and the three-order-of-magnitude change in $L$ allow a clear separation of the surface and gas contributions.

The surface that is plotted in Fig. 14 is given by

$$L = L_g e^{\zeta(B-7.62)} + L_s \frac{A}{V} \Lambda^3 e^{\zeta(B-7.62)} e^{3E_b/k_B T} . \tag{58}$$

The parameters which were fit are the binding energy $E_b$, the strength of the magnetic field dependence $\zeta$, and the volume and surface three-body recombination constants $L_g$ and $L_s$.

#### 1. Binding energy

Our result for the binding energy of H on $^4$He is $E_b/k = 1.04(3)$ K. This value is about midrange among the values by other techniques.[11] This method of determining $E_b$ has the advantage of high sensitivity. It has the disadvantage that it relies on an assumption about the temperature dependences of $L_g$ and $L_s$ (see Table III).

TABLE III. The effect of several hypothetical temperature dependences of $L_g$ and $L_s$ on the results of a 4 parameter fit to the data in Fig. 14 (76 degrees of freedom, 4 priameters).

| $L_g$ ($\mathrm{cm^6 s^{-1}}$) | $L_s$ ($\mathrm{cm^4 s^{-1}}$) | $E_b$ (K) | $\zeta$ ($\mathrm{T^{-1}}$) | $\chi^2/n$ |
|---|---|---|---|---|
| $8.9\times10^{-39}$ | $1.2\times10^{-24}$ | 1.04 | −0.07 | 1.50 |
| $8.6\times10^{-39}$ | $1.0\times10^{-24}\times(T/0.5\ \mathrm{K})^{1/2}$ | 1.08 | −0.07 | 1.54 |
| $8.1\times10^{-39}\times(T/0.5\ \mathrm{K})^{1/2}$ | $1.9\times10^{-24}$ | 0.99 | −0.07 | 1.58 |
| $8.9\times10^{-39}\times(T/0.5\ \mathrm{K})^{1/2}$ | $1.5\times10^{-24}\times(T/0.5\ \mathrm{K})^{1/2}$ | 0.99 | −0.06 | 1.51 |
| $8.6\times10^{-39}$ | $7.0\times10^{-25}\times(T/0.5\ \mathrm{K})$ | 1.15 | −0.07 | 1.58 |
| $8.0\times10^{-39}\times(T/0.5\ \mathrm{K})^{-1/2}$ | $1.4\times10^{-24}$ | 1.05 | −0.07 | 1.79 |

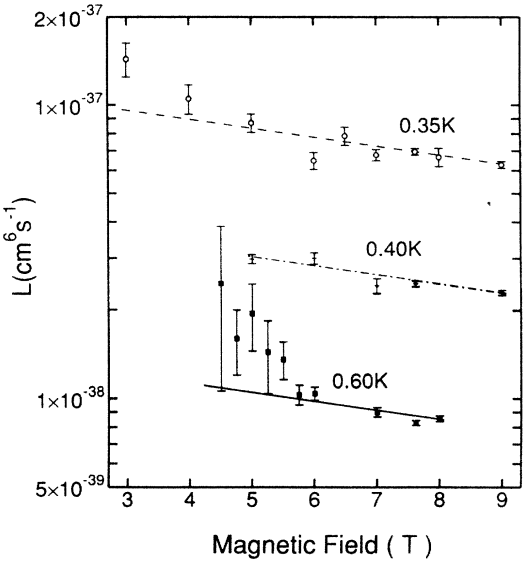


FIG. 16. Magnetic field dependence of the three-body recombination rate constant $L$. Circles, crosses, and squares correspond to $T=0.35$, 0.40, and 0.60 K, respectively. The lines show our fit of the data to Eq. (58). At 0.35 K, $L$ is dominated by a surface process, while at 0.60 K, recombination in the gas dominates.

### 2. *Magnetic field dependence of $L_g$ and $L_s$*

The magnetic field dependence of $L$ is shown in Fig. 16. Kagan *et al.*[8] predicted that the dipole three-body recombination should be strongly field dependent. They calculated that $L_g$ would increase by a factor of 3 between 5 and 10 T, in marked contrast to the weak decrease which we observe. A recent calculation by de Goey, Driessen, Verhaar, and Walraven[31] predicts a field dependence which is only slightly weaker than that of KVS.[8]

We have parametrized the field dependence that we observe by a factor of $e^{\zeta(B-7.62)}$, where $B$ is in tesla and $\zeta$ is a small number. We expect the field dependence of the surface and volume three-body recombination coefficients, $L_s$ and $L_v$, to be similar because the surface plays no essential role in the recombination mechanism. Further, the bound state on the surface extends to a distance significantly greater than the hard core radius of a hydrogen atom, so that the interactions of atoms in the surface bound state should have an approximately three-dimensional character.[30] When $\zeta_g$ and $\zeta_s$ were varied independently we obtained $\zeta_g=-0.06(2)$ T$^{-1}$ and $\zeta_s=-0.07(2)$ T$^{-1}$. However, the significance of this small difference is questionable. Fits of equal quality we obtained when $\zeta_g$ and $\zeta_s$ were constrained to be equal, resulting in the quoted value $\zeta=-0.07(2)$ per tesla.

One possible explanation of the unexpected field dependence of $L$ is associated with a nonthermal distribution of atomic kinetic energies in the gas due to the recombination events. This mechanism is discussed in Appendix C. However, we believe that it does not influence our results at the densities where data was extracted, though it could play a role at densities above $n=10^{18}$ cm$^{-3}$.

### 3. *Temperature dependence of $L_g$ and $L_s$*

In carrying out our fits we have assumed that $L_g$ and $L_s$ were independent of temperature. Due to the presence of the strongly temperature dependent exponential term in Eq. (32), it is difficult to obtain information about a possible weak temperature dependence of $L_g$ or $L_s$. Table III shows how the results of the fit change when several representative temperature dependences are assumed for $L_g$ and $L_s$.

### 4. *Three-body dipolar recombination in the gas*

Our result at $B=7.6$ T is $L_g=8.9(8)\times10^{-39}$ cm$^6$s$^{-1}$. This is about twice the value $4(2)\times10^{-39}$ cm$^6$s$^{-1}$ reported by Sprik, Walraven, and Silvera[9] at 0.75 K and 9.8 T. They have recently found a correction to their initial analysis and now report a value of $7(2)\times10^{-39}$ cm$^6$s$^{-1}$.[57]

For a field of 10 T, KVS (Ref. 8) calculated $C_g^d=3.4\times10^{-39}$ cm$^6$s$^{-1}$. For the conditions of our experiments, their expressions predict $2+2N^d=3.9$, with the result that $L_g=1.3\times10^{-38}$ cm$^6$s$^{-1}$, somewhat larger than our measured value at $B=7.62$ T. The calculation by de Goey *et al.*[31] is in reasonable agreement with the KVS results in the gas. Their expressions correspond to $C_g^d=4.3\times10^{-39}$ cm$^6$s$^{-1}$ at $B=10$ T.

### 5. *Three-body recombination on the surface*

Assuming that $L_s$ is temperature independent, our result at $B=7.6$ T is $L_s=1.2(4)\times10^{-24}$ cm$^4$s$^{-1}$. To investigate this assumption, Table III contains fits made with other assumed temperature dependences. Reynolds *et al.*[55] recently observed three-body surface recombination by ESR in the temperature range 0.1 K $<T<$0.2 K at a field of 4.1 T. They state that their result for $L_s$ is consistent with our results[12] but do not quote a value from their experiment.

The surface three-body rate was first discussed by KVS (Ref. 8) and an improved estimate, Eq. (27), has been given by Kagan *et al.*[30] Equation (27), evaluated with the value of Kagan *et al.* of $l=4.8$ Å, predicts $(L_g/L_s)^{1/2}=4\times10^{-8}$ cm. This is fairly close to our measured ratio of $8.6(12)\times10^{-8}$ cm. (The discussion below on results for $^3$He surfaces will comment further on this.) On the other hand, the calculation of de Goey *et al.*[31] (assuming $2+2N^d=3.9$) gives $L_s=2.5\times10^{-25}$ cm$^4$s$^{-1}$ for a magnetic field of $B=7.6$ T normal to the surface, which is a factor of 5 less than our measured value under these conditions.

### 6. *Angular dependence of $L_s$*

It is now clear that earlier noncompression observations of H↓ decay were strongly affected by surface three-body recombination (see Appendix B). This contention can be demonstrated[14] by reanalyzing one of the sets of data originally taken[6] to study nuclear relaxation. These data were taken in a cell whose walls were predominantly parallel to the magnetic field, whereas in our present cell, 96% of the wall area is perpendicular to the field. A comparison of data from these two cells can give information on the an-

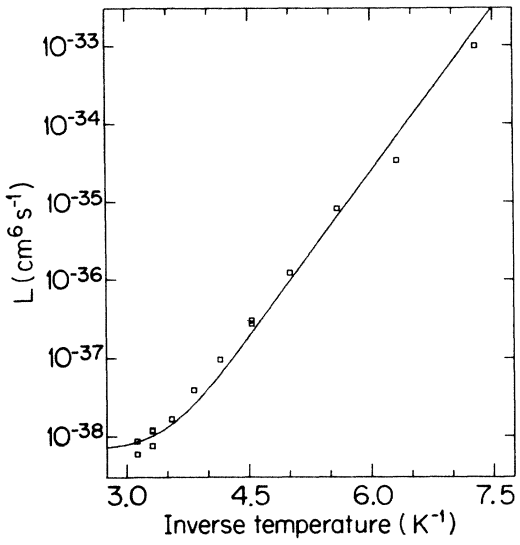


FIG. 17. Values of $L$ obtained by a reanalysis Ref. 6 data (circles) obtained in a cell with the magnetic field predominantly parallel to the surface ($B=11$ T). The solid line is a plot of $L$ extrapolated from recent compression experiments with the magnetic field predominantly perpendicular to the surface.

gular dependence of $L_s$. It should be noted that although a "muffin-tin" model for microscopic surface roughness has been used in discussions of angular dependence,[27,53] we do not believe it applies in our case. We have inspected the surfaces of our cell with a scanning electron microscope, and find that typical microscopic irregularities are significantly smaller than the $5\mu$ capillary radius [Eq. (38)] of the $^4$He in our cell.

The temperature dependence of $L$ in the earlier measurement, Ref. 6, is shown in Fig. 17. Because the cell was open in those experiments, the $c$-state atoms generated by three-body recombination could be expelled from the cell by the magnetic field gradients before recombining with a fourth atom. To compare those results with the current measurements, a correction must be made for this possible loss of atoms. We have modeled the diffusion of $c$-state atoms out of the cell, and calculated probabilities of escape and relaxation. The probability of escape was found to vary from 0.5 at our highest density to 0.998 at the lowest density. The probability of relaxation from the $c$ state to the lower two hyperfine states was less than 0.08. Consequently, the mean number of atoms removed per event varied from $2.94<\lambda<3.30$. The data were then scaled to $N^d=0.93$, as would be valid in a closed cell. The solid line on Fig. 17 shows the value of $L$ versus $T^{-1}$ that would be expected by extrapolating Eq. (58) using the values of $L_g$, $L_s$, and $\zeta$ repeated above. The agreement is good, though some deviation at low temperatures is apparent, probably due to difficulties in thermometry in the older data.

We conclude that $L_s$ is not strongly anisotropic unless the angular dependence is coincidentally canceled by its field dependence in the region $9\text{ T}<B<11$ T. The lack of a significant angular dependence of $L_s$ is consistent with the theoretical predictions of de Goey *et al.*[31]

*7. Three-body recombination due to electron depolarization*

At low magnetic fields and high temperatures, electronic relaxation can cause depolarization by promoting atoms from the $b$ to the $c$ state. Most of these $c$ atoms recombine on the walls, contributing to the two-body decay of the sample shown in Fig. 12. However, some of them can recombine in a three-body gas event. In an earlier publication[14] we proposed a mechanism by which these three-body events would give a separate, additive contribution to our measured three-body rate constant $L$. Such a contribution appeared to be present in our data. Subsequently Sprik pointed out to us that a complete treatment of the mechanism we proposed effected $L$ only in second order, causing a change too small to explain our observed increase in $L$. A reexamination of the influence of electronic relaxation on the dynamics of the decay [see Eq. (45)] resolved the discrepancy. Computer generated model decays showed that when the nuclear polarization differed substantially from $-1$ (that is at high temperature and low magnetic fields), the electronic relaxation caused $-\dot{n}/n^2$ versus $n$ to have a finite slope, even in the absence of three-body processes. It was this slope which we mistook for a three-body mechanism involving the finite $c$-state density. Reanalysis of our data using more realistic models now shows that the low-field, high-temperature data does not allow a determination of the rate constants for the $b+b+c\rightarrow H_2+X$ and related processes.

C. Measurements of $L_s$ and $E_b$ for $^3$He-$^4$He solutions

$^3$He has a smaller mass than $^4$He. As a result its zero-point motion is larger, its atomic density is lower and its liquid presents a smaller van der Waals attraction for atomic hydrogen. Consequently, the binding energy of H on a surface of $^3$He is significantly lower than it is on $^4$He. Jochemsen *et al.*[46] report $E_b/k=0.42(5)$ K based on NMR measurements in unpolarized H. (This is to be compared with $E_b/k\approx 1$ K for $^4$He.) The low binding energy makes $^3$He an attractive medium for the surfaces of a confinement cell. Unfortunately, H↓ has yet to be stabilized in a cell with pure $^3$He surfaces. A major difficulty compared to $^4$He is the lack of the self-healing properties of a superfluid film. Van Yperen *et al.*[59] stabilized H↓ using concentrated $^3$He-$^4$He solutions and determined the binding energy under these conditions to be 0.34(3) K. It is puzzling that this value is less than that for pure $^3$He, for simple polarizability arguments dictate that $E_b$ should decrease monotonically with increasing $^3$He concentration.

In these experiments we have examined two concentration regimes: the first corresponds to a monolayer of $^3$He on the surface on the $^4$He, the second to an 8% solution of $^3$He.

Carrying out experiments with $^3$He-$^4$He solutions presents new experimental problems. The surface tension of the solutions is less than that of pure $^4$He,[60] making it difficult to seal the piston during compression and to maintain the seal during the decay. The sample chamber is not closed for the $^3$He atoms because they can diffuse in the liquid past the piston into the remainder of the apparatus. Sudden jumps in the decay rate of the hydrogen sometimes occurred during a trace. We attribute these to

changes in the $^3$He concentration in the sample chamber driven by osmotic pressure gradients due to temperature changes in other parts of the cell.

Figure 18 shows $-\dot{n}/n^2$ for a decay taken at a $^3$He concentration $X \equiv n_3/(n_3+n_4) = 1.5\times10^{-4}$ and temperature 0.20 K. The single bound state for $^3$He at the surface of the liquid has an energy of $-2.2$ K relative to $^3$He atoms dissolved in the bulk liquid.[59] The temperature and concentration at which the data were taken assure that the surface state is completely occupied, giving rise to a completed monolayer of $^3$He at a density estimated to be about $6\times10^{14}$ atoms cm$^{-2}$. The three-body rate coefficient determined from the trace is $L \approx 2\times10^{-37}$ cm$^6$s$^{-1}$. This is 500 times smaller than the value which would be obtained for pure $^4$He surfaces at the same temperature and field. If one assumes that the three-body surface rate constant $L_s$ has not changed from its $^4$He value, Eq. (33) gives a value of $E_b/k \approx 0.6$ K under these conditions. These values are consistent with data obtained from other traces taken at $X = 1.5\times10^{-4}$. The conclusion is that even a monolayer of $^3$He has a marked effect on the $H_\downarrow$ binding energy. This is consistent with earlier results by Matthey *et al.*[5] on less well characterized films.

Figure 19 shows the temperature dependence of $L$ for solutions at a $^3$He concentration $X = 8.0\times10^{-2}$. For most values of the temperature there is no phase separation in the saturated film but the surface $^3$He monolayer is completed. At the two lowest temperatures, however, phase separation is predicted on the basis of the known properties of the bulk film. The concentrated $^3$He phase should be farthest from the wall. Although the traces from which this data were obtained were better than that shown for low concentrations in Fig. 18, they lacked the quality and high degree of reproducibility characteristic

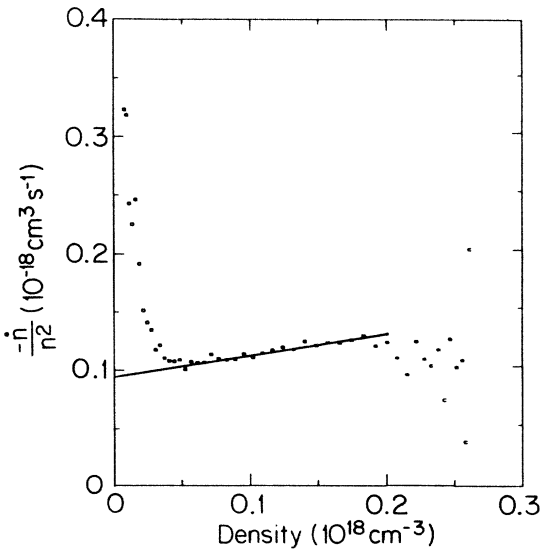


FIG. 18. Experimental results for a decay with a $^3$He concentration $X = 1.5\times10^{-4}$, temperature 0.20 K, and magnetic field 9 T. The rise of $-\dot{n}/n^2$ at low densities is due to drifts of the baseline and concentration, rather than to a one-body process. The solid line has a slope of $L = 2\times10^{-37}$ cm$^6$s$^{-1}$.

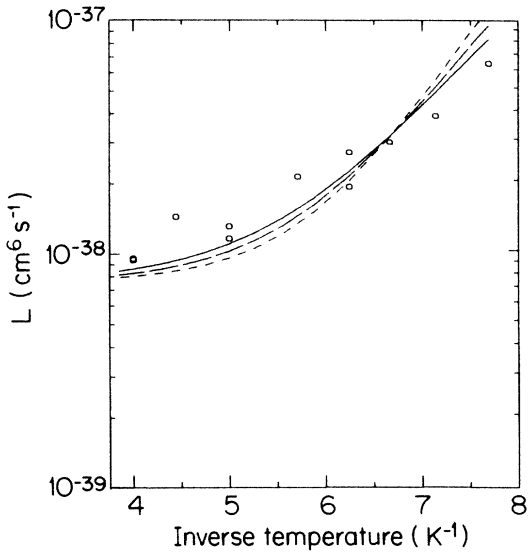


FIG. 19. Temperature dependence of $L$ for solutions with a $^3$He concentration $X = 0.08$ at a magnetic field $B = 7.6$ T. The lines indicate the results of one parameter fits to the data. Solid line: $L_g$ was held fixed at the value obtained for pure $^4$He ($2.0\times10^{-24}$ cm$^4$s$^{-1}$); $E_b$ was determined to be 0.31 K. Short dashed line: $E_b$ fixed at 0.42 K; $L_s$ determined to be $0.2\times10^{-24}$ cm$^4$s$^{-1}$. Long dashed line: $L_s$ proportional to $E_b$ yields $E_b = 0.36$ K and $L_s = 0.7\times10^{-24}$ cm$^4$s$^{-1}$.

of the decays with pure $^4$He. However, the use of $^3$He-$^4$He solutions allowed us to compress $H\downarrow$ to much higher densities at low temperature than was possible with pure $^4$He. For example with the 8% solution we were able to attain a density $n = 3.1\times10^{18}$ atoms cm$^{-3}$ at a gas temperature $T = 0.38$ K and $n = 1.4\times10^{18}$ atoms cm$^{-3}$ at $T = 0.19$ K.

The great reduction in $L$ achieved at low temperatures by using $^3$He-$^4$He solutions can be appreciated by comparing Fig. 19 with the pure $^4$He values in Fig. 15. Note that the data for solutions begin at a temperature of 0.25 K, whereas the data for pure $^4$He terminates at 0.25 K because the decay becomes too rapid to measure accurately. Unfortunately, the scatter in the data of Fig. 19 is too large to allow $L_s$ and $E_b$ to be determined separately. To determine $E_b$ from the data we have employed Eq. (32) using the value of $L_g$ obtained from the measurements with pure $^4$He. Taking $L_s = 2.0\times10^{-24}$ cm$^4$s$^{-1}$, the best fit to the data is $E_b/k = 0.31$ K. This is smaller than either of the two previously reported values. Alternatively, if one assumes $E_b/k = 0.42$ K—the result obtained by Jochemsen *et al.*[46] for pure $^3$He—one obtains $L_s = 0.2\times10^{-24}$ cm$^4$s$^{-1}$, and a noticeably poorer fit to the data.

Kagan *et al.*[30] argue that the localization distance $l$ of adsorbed H atoms perpendicular to the surface should vary as $E_b^{-1/2}$. Then, by Eq. (27), the three-body dipole surface rate coefficient should be directly proportional to $E_b$. We have tried a one parameter fit to the data of Fig. 19 using the constraint $L_s(X=0.08)/L_s(X=0.0) = E_b(X=0.08)/E_b(X=0.0)$. The results were $L_s(X=0.08) = 0.73\times10^{-24}$ cm$^4$s$^{-1}$ and $E_b(X=0.08)/$

$k=0.36$ K. The quality of the fit falls between that of the other two cases, as shown in Fig. 19. More quantitative results will require better control and measurement of the $^3$He concentration.

## ACKNOWLEDGMENTS

This work was supported by the National Science Foundation through Grant Nos. DMR-8304888 and DMR-8513769. One of us (G.P.K.) would like to acknowledge the support of AT&T Bell Laboratories.

## APPENDIX A: DELAYED RECOMBINATION

In this section we examine the fate of a $c$ atom immersed in a gas of $b$ atoms. We will show that under the conditions of these experiments the $c$ atom is much more likely to recombine and to remove two atoms from the system, than to relax to the $b$ state which would not decrease the number of atoms. Numerical values for rate constants involving $d$ atoms are expected to be similar, and the same conclusions should hold.

### 1. Spin relaxation in the gas

In this process the $c$ atom relaxes back to the $b$ state due to the time varying magnetic fields generated by the random motion of the other atoms in the gas.

$$\dot{n}_c = -G_{bc,bb} n_c n_b \ . \tag{A1}$$

The reverse of this process, the promotion of atoms from $b$ to $c$, was discussed in Sec. II D. The rates for the processes differ by the factor $\exp(-2\mu B/k_B T)$. Our measurements give the value $G^{cb}=G_{bc,bb}=1.2\times10^{-15}$ cm$^3$s$^{-1}$. The resulting relaxation time is

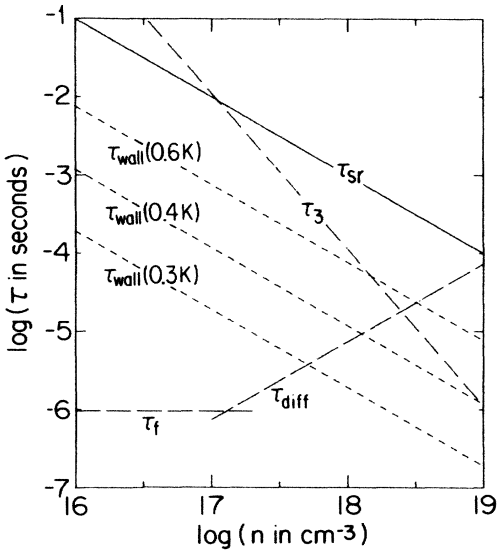


FIG. 20. Times associated with the fate of a $c$-state atom in a cell filled with $b$-state atoms. $\tau_{sr}$ is the spin relaxation time, $\tau_3$ is the three body recombination time, $\tau_f$ is the flight time to the wall in a low-density gas, $\tau_{\rm diff}$ is the diffusion time to the wall at high densities, and $\tau_{\rm wall}$ is the recombination time on the wall.

$$\tau_{sr} \equiv (-\dot{n}_c/n_c)^{-1} = (G^{cb} n_b)^{-1} \ . \tag{A2}$$

$\tau_{sr}$ will serve as a reference time; all steps involved in the recombination process must be faster than this if the $c$ atom is to recombine before it relaxes to the $b$ state. $\tau_{sr}$ is plotted as a function of the density of $b$-state atoms in Fig. 20.

### 2. Three-body recombination in the gas

The Kagan mechanism is not invoked here since the $c$ atom is already depolarized:

$$\dot{n}_c = -K_{bbc} n_c n_b^2 \ . \tag{A3}$$

This is the simplest recombination process since it is not mediated by the wall. $K_{bbc}$ has not been measured directly, but it should be comparable to the value $K^{(3)}_{\rm He}=2.0\times10^{-33}$ cm$^6$s$^{-1}$ found by Morrow[61] for the reaction $H + H + He \rightarrow H_2 + He$:

$$K_{bbc} \sim \xi K^{(3)}_{\rm He} \tag{A4}$$

where $\xi$ is a dimensionless factor somewhat greater than unity due to the increased probability of singlet pairing in the all-hydrogen reaction. We have used $\xi=4$ to plot the resulting recombination time,

$$\tau_3 \equiv (-n_c/n_c)^{-1} = (K_{bbc} n_b^2)^{-1} \tag{A5}$$

in Fig. 20. The result shows that if one had to wait for this process to cause recombination, the $c$ atom would have a good chance of relaxing instead. However, as described below, two-body recombination on the wall occurs at a much faster rate.

### 3. Transit time to the wall

Assuming thermal equilibrium and no collisions, the mean flight time of an atom to the wall is

$$\tau_f = \frac{1}{2} w \langle v_x \rangle^{-1} = \frac{1}{2} w \left[ \frac{2k_B T}{\pi M} \right]^{-1/2} , \tag{A6}$$

where $w$ is the cell thickness. This is plotted in Fig. 20 using our value $w=7.5\times10^{-3}$ cm and a temperature of 0.3 K. At high densities the time the $c$ atom takes to reach the wall is limited by collisions with the $b$ atoms. We define a characteristic time $\tau_{\rm diff}$, the time required for perfectly absorbing walls to remove half of an ensemble of $c$ atoms that are assumed to be uniformly distributed in the cell at $t=0$.[62]

$$\tau_{\rm diff} = 0.197 \frac{w^2}{D} \ , \tag{A7}$$

where $D$ is the diffusion constant for the $c$ atoms in the $b$-state gas. A good approximation to the particle diffusion coefficient $D$ is $\mathscr{D}$, the transverse spin diffusion coefficient in unpolarized atomic hydrogen. Lhuillier[52] has calculated this quantity and finds $\mathscr{D}\rho \approx 2.5\times10^{-7}$ m$^{-1}$kg s$^{-1}$ in our temperature region, which is equivalent to $\mathscr{D} n = 1.5\times10^{18}$ cm$^{-1}$s$^{-1}$. We have used this result in plotting the characteristic diffusion time to the wall, Eq. (A7), on the graph in Fig. 20. The diffusion result no longer holds when the mean free path $\lambda$ approaches the

cell width $w$. Note that the curves for $\tau_f$ and $\tau_{\rm diff}$ intersect close to the density ($1.5\times10^{17}$ cm$^{-3}$) at which $\lambda=w/2$. $\lambda$ was computed from the simple kinetic theory expression

$$\lambda\approx\frac{3\mathscr{D}}{\langle v\rangle}=3\mathscr{D}\left[\frac{8k_BT}{\pi M}\right]^{-1/2}. \tag{A8}$$

#### 4. Time required to establish equilibrium between bulk and surface

The sticking probability $s$ for hydrogen atoms hitting the helium surface is less than unity; thus, the $c$ atoms which reach the wall may have to collide with the surface many times before being adsorbed. One may estimate the time needed for the surface density of $c$ atoms to come to equilibrium with the bulk density as follows. Assume a density $n_c$ of $c$ atoms in the gas next to an unoccupied surface. The rate at which $c$ atoms would be adsorbed onto the surface is $\gamma_A=s\gamma_C$ where $\gamma_C=n_c\langle v\rangle/4$ is the rate of $c$-atom collisions with the surface. Eventually the surface density reaches its equilibrium value $\sigma(T)$ and atoms leave the surface as rapidly as they are adsorbed. The time required to reach equilibrium is then roughly $\tau=\sigma/\gamma_A$. Substituting expressions for $\sigma(T)$, $\gamma_C$, and $\langle v\rangle$ gives the strongly temperature-dependent result:

$$\tau_{ads}=\frac{\Lambda(T)}{s}\left[\frac{k_BT}{2\pi M}\right]^{-1/2}e^{E_b/k_BT}. \tag{A9}$$

Using the value $s=0.046$ measured by Morrow *et al.*[4] and a surface binding energy $E_b=1.0$ K, this time is only $9.7\times10^{-8}$ s at $T=0.3$ K. For higher temperatures, it is even shorter. This time is too short to be plotted in Fig. 20.

#### 5. Recombination on the walls

The $c$-state atoms which adsorb on the walls give rise to a two-body recombination process:

$$\dot{n}_c=-K^{bc}n_cn_b\ . \tag{A10}$$

The effective volume recombination coefficient $K^{bc}$ is from Eq. (16). Morrow *et al.*[4] have measured $K_s(B=0)$ and present their results in terms of a "cross-length," $\langle l\rangle$, as defined in Eq. (10). Their value $\langle l\rangle=0.14$ Å on a $^4$He surface leads us to the result $K_s^{bc}=4.5\times10^{-5}$ (T/1 K)$^{1/2}$cm$^2$s$^{-1}$. The corresponding time for the $c$-state gas density to decrease due to surface recombination is

$$\tau_{\rm wall}^{-1}=K_s^{bc}n_b\frac{A}{B}\Lambda^2(T)e^{2E_b/k_BT} \tag{A11}$$

is plotted in Fig. 20 for the range of temperatures used in these experiments.

Figure 20 shows that the $c$-state recombination time is at least an order of magnitude shorter than the relaxation time $\tau_{sr}$ [Eq. (A2)] and considerably longer than the times necessary to get to and onto the surface. This shows that for $T<0.6$ K, virtually all $c$ atoms recombine before they relax. For $T=0.6$ K, relaxation should not have a large effect on the decay. However, to complete the argument, two additional processes should be mentioned.

#### 6. Relaxation on the wall

There have been no calculations of the electron spin-relaxation rate on surfaces similar to the calculation in the bulk carried out by KVS. However, the similarity between nuclear and electronic relaxation mechanisms in H allows us to carry out a crude estimate simply by scaling the calculated nuclear relaxation rate coefficient on the wall by the ratio of the measured electronic and nuclear rate coefficients in the gas:

$$G_s^{cb}\approx G_s^{ba}(G^{cb}/G^{ba})\ . \tag{A12}$$

The experimental results reported for the gas in Sec. VI give $(G^{cb}/G^{ba})=1.8\times10^5$. Using the theoretical value $G_s^{ba}(45°)=8\times10^{-14}$ cm$^2$s$^{-1}$ from Eq. (21) leads to the estimate $G_s^{cb}\approx10^{-8}$ cm$^2$s$^{-1}$. Converting this to an effective bulk rate coefficient by an expression similar to Eq. (13) gives $G_{\rm eff}^{cb}\approx3\times10^{-16}$ cm$^3$s$^{-1}$. This is less than the direct bulk relaxation rate coefficient used in Eq. (A2). Furthermore, the angular dependence of $G_s^{cb}$, if similar to that of the nuclear relaxation, would further suppress the surface rate in our geometry.

#### 7. Spin exchange

Atoms can leave the $c$ state due to spin-exchange collisions.[63]

$$c+a\rightarrow d+b \tag{A13}$$

and this process is sufficiently fast to maintain $n_an_c=n_dn_b$. This does not affect the above conclusions; as it merely exchanges one upper-state atom for another. The recombination and relaxation rates for $d$ atoms are close to the corresponding processes involving $c$ atoms. It has a somewhat more subtle effect: as $c$- and $d$-state atoms interconvert before recombining, they transfer atoms between the $a$ and $b$ states, thus affecting the nuclear polarization.

## APPENDIX B: REINTERPRETATION OF SURFACE NUCLEAR RELAXATION DATA

We have concluded from these experiments that the parameter for the surface two-body relaxation rate coefficient $G_s^{ba}$ is less than $2\times10^{-13}$ at 8 T (see Sec. VI A), consistent with theoretical calculations. Earlier reported experimental values[6,16,19] on the order of $G_s^{ba}=7\times10^{-13}$ cm$^2$s$^{-1}$, about 50 times the theoretical calculations. We now understand how this discrepancy arose, at least in the case of our own measurements. The reason $G_s^{ba}$ was thought to be important has to do with the way experiments were done before compression techniques were developed. In our case, the sample cell would be filled for 10 min, reaching a density of about $10^{17}$ atoms/cm$^3$ at 0.3 K, and a somewhat lower density at lower temperatures. At that point the polarization of the gas would be quite low; after turning the discharge off we waited till the decay rate slowed down, indicating that nuclear polarization had been achieved. Then the quantity $-\dot{n}/n^2$ would be computed, but it was not plotted over a wide range of density as we have done here. At the low temperatures it was

assumed to have a contribution $G_s^{ba}(\sigma/n)^2$ which agreed with the observed temperature dependence, $\exp(2E_b/k_BT)$. If the effect was caused by three-body recombination, the contribution to $-\dot{n}/n^2$ would be $nL_s(\sigma/n)^3=\sigma L_s(\sigma/n)^2$. We have reexamined the original data and determined that the gas densities at which "$G$" was measured decreased in such a way that $\sigma$ was roughly constant (see Fig. 2 of Ref. 13).

This arose because the initial density for a trace was determined by a balance between a constant filling flux and a decay rate governed by the surface density. With $\sigma$ as a constant, the $L_s$ contribution to $-\dot{n}/n^2$ would also be proportional to $\exp(2E_b/k_BT)$, and display the signature of two-body surface relaxation. Under these conditions, one can not distinguish between $G_s$ and $L_s$ by their temperature dependence. We conclude that the large experimental values formerly attributed to $G_s$ are in error and that the effect was due instead to surface three-body recombination.

## APPENDIX C: NONTHERMAL ENHANCEMENT OF RECOMBINATION

The energy released by a recombination event can lead to further recombination as in the thermal explosion process predicted by Kagan[39] and observed in several laboratories.[9,12,38] In this process, the thermalized heat of recombination increases the temperature-sensitive electron depolarization rate leading to further recombination and possibly an explosion. In this appendix, we examine a similar process involving *nonthermalized* energy of recombination that could modify the interpretation of the three-body rates. A simple explanation of this nonthermal electron depolarization is presented. We conclude that the effect does not play a role in the results quoted in the body of the paper, but that it must be taken into account in experiments at high densities or in other geometries.

Each recombination event creates a molecule in a high vibrational and rotational state. As this molecule cascades to the ground state, a fraction of its energy $(1-\xi)D_0$ is dissipated in the liquid helium walls, while the remainder $\xi D_0$ generates a non-thermal distribution of hydrogen atom energies. Each recombination event can produce $\xi D_0/E_k$ hydrogen atoms with a kinetic energy of $E_k$. Atoms which are only a few collisions removed from an inelastic encounter with the excited $H_2$ molecule will have energies well above $k_BT$. They form an excess population of density $n_>(E_k)$ superimposed on the high-energy Boltzmann tail. One would expect

$$n_>(E_k)=-\frac{1}{2}\frac{dn}{dt}\xi\frac{D_0}{E_k}\tau\psi\ , \tag{C1}$$

where $\tau=1/\bar{v}n\sigma_0$ is the mean collision time, $(1/2)(dn/dt)$ is the rate of formation of molecules, and $\psi$ is a dimensionless coefficient of order unity.

Electron relaxation to the $c$ state is enhanced for collisions involving these energetic ($E_k\geq 2\mu B$) $b$-state atoms since the thermal activation exponent $e^{-2\mu_B B/k_BT}$ does not suppress the rate. This relaxation process occurs via two channels[8] at a rate five times that of our measured $G_v^{bc}$. The new expression for recombination is

$$\frac{dn}{dt}=-2Gn^2-2(1+N^d)C^dn^3-5.2\times G_v^{bc}nn_>(2\mu B)\ , \tag{C2}$$

or

$$\frac{dn}{dt}=(2Gn^2+2(1+N^d)C^dn^3)\Gamma\ , \tag{C3}$$

$$\Gamma=\left[1-\frac{5}{2}\frac{G_v^{bc}\xi\psi D_0}{\bar{v}\sigma_0\mu B}\right]^{-1}\ . \tag{C4}$$

$\Gamma$ is a dimensionless enhancement factor due to the nonequilibrium energy distribution.

The fraction of energy released to the gas $\gamma$ should be strongly density dependent—large at high gas densities where the mean free path is small compared to sample dimensions, and vanishingly small at low densities. (Our sample is one mean free path thick at $n=8\times10^{16}$ cm$^{-3}$.) Our two- and three-body rates are determined from the low-density limit of the data where the prefactor $\Gamma$ can be expected to approach unity.

The situation is different for densities above $10^{18}$ cm$^{-3}$. A value of $\Gamma$ greater than unity would have two consequences. First the measured rates $G$ and $L$ would appear larger than the rates appropriate at low densities. Second, the apparent field dependences of $G$ and $L$ would be modified. In the case of $L$, Eqs. (29), (31), and (32) would be replaced by

$$L(B)=\Gamma(B)2(1+N^d)C^d(B)\ . \tag{C5}$$

Our measured field dependence of $G^{ba}$ is in excellent agreement with theory, implying that $\Gamma(B)$ is close to unity for the density region where the data was most sensitive to $G$. The $L$ values, however, were determined from slightly higher density regions of the decays. An important unresolved issue is the difference between the field dependences of the experimental and theoretical three-body rates. The rate coefficient $L(B)$ was found to decrease with field at 7% per tesla while theoretical work predicts the three body event rate $W_g^d(B)$ to increase at 25% per tesla[8] or 10% per tesla.[31] The multiplicative factor $\Gamma(B)$ has a negative field dependence which could resolve the discrepancy if $\Gamma(6\text{ T})$ were 2.9 or 2.0, respectively. However, this is not the case for our data. The density used in the determination of the three-body rates was usually below $5\times10^{17}$ cm$^{-3}$, in the limit where $\Gamma\approx1$. Furthermore, this enhancement effect gives rise to a nonlinear dependence on density as one goes between the low-density $\Gamma\approx1$ and the high-density $\Gamma>1$ regions; no such anomaly was observed below $5\times10^{17}$ cm$^{-3}$.

In order to assess the importance of this nonthermal enhancement at higher densities a more quantitative understanding of the nonthermal distribution and the mechanisms by which it dissipates energy is required. This would give both the coefficient $\psi$ and the fraction $\gamma$ as a function of density. This process might be important at densities over $1\times10^{18}$ cm$^{-3}$ in our compression cell or in larger geometries used in the recent bubble compression experiments[9,38] and perhaps the older continuous fill cells.

## APPENDIX D: GLOSSARY OF FREQUENTLY USED SYMBOLS

In this glossary superscript or subscript Greek letters stand for arbitrary hyperfine states.

| Symbol | Section | Units | Meaning |
|---|---|---|---|
| $\alpha$ | V B 2 [Eq. (50)] | | Accommodation coefficient |
| $\Gamma$ | Appendix C | | Enhancement due to nonthermal distribution |
| $\Gamma_s^{ba}$ | VI A | | Fitting parameter for surface nuclear relaxation |
| $\theta$ | II A | | Hyperfine mixing angle |
| $\sigma$ | II B | $cm^{-2}$ | Surface density |
| $\dot{\sigma}$ | II B | $cm^{-2}s^{-1}$ | A contribution to the recombination rate from the surface |
| $\Lambda(T)$ | II B [Eq. (12)] | cm | Thermal deBroglie wavelength of H |
| $\gamma$ | II B | | $K_{aa}/K_{ab}$ |
| $\mu_B$ | II A | $erg\,T^{-1}$ | Bohr magneton |
| $\kappa$ | V B 2 | $erg\,K^{-1}\ cm^{-1}s^{-1}$ | Thermal conductivity of H gas |
| $\varphi$ | VI A | | Fitting parameter for volume nuclear relaxation |
| $\zeta$ | VI B | $T^{-1}$ | Fitting parameter for field dependence of $L$ |
| $dn/dt$ | II B | $cm^{-3}s^{-1}$ | Rate of change of density |
| $a,b,c,d$ | II A | | Hyperfine states of hydrogen |
| $A$ | II B | $cm^2$ | Surface area of sample cell |
| $B$ | | T | Magnetic field strength in the sample |
| $C_g^{ex}$ | II E [Eq. (25)] | $cm^6s^{-1}$ | Three-body exchange rate constant |
| $C_g^d$ | II E [Eq. (26)] | $cm^6s^{-1}$ | Three-body dipole-dipole rate constant |
| $C_s^d$ | II E [Eq. (26)] | $cm^4s^{-1}$ | Three-body surface dipole-dipole rate constant |
| $C^{\alpha\beta\gamma}$ | II E [Eq. (28)] | $cm^6s^{-1}$ | A specific three-body recombination rate constant |
| $D_0$ | II B | erg | Dissociation energy of $H_2$ |
| $E_b$ | II B | erg | Binding Energy of H to a He film |
| $E_{\alpha\beta}$ | II C | erg | Energy difference between two hyperfine states |
| $F(B)$ | II C [Eq. (20)] | | Field dependence of nuclear relaxation rates |
| $G_{\beta\gamma,\theta\sigma}$ | II C | $cm^3s^{-1}$ | A specific relaxation rate constant |
| $G^{ba}$ | II C | $cm^3s^{-1}$ | Nuclear relaxation rate constant |
| $G_s^{ba}$ | II C | $cm^2s^{-1}$ | Surface nuclear relaxation rate constant |
| $G^{bc}$ | II D [Eq. (23)] | $cm^3s^{-1}$ | Electronic relaxation rate constant |
| $G^{cb}$ | II D [Eq. (24)] | $cm^3s^{-1}$ | Electronic relaxation rate constant |
| $g^{bc}$ | V B 1 | $cm^3s^{-1}$ | Parameterization of $G^{bc}$ |
| $H_\downarrow$ | II A | | Electron-polarized hydrogen |
| $H_{\downarrow\mp}$ | II A | | Electron and nuclear polarized hydrogen |
| $j_g$ | V B 3 | $erg\,cm^{-2}s^{-1}$ | Heat flux from recombination in the gas |
| $j_u$ | V B 3 | $erg\,cm^{-2}s^{-1}$ | Heat flux from recombination on the upper surface |
| $j_l$ | V B 3 | $erg\,cm^{-2}s^{-1}$ | Heat flux from recombination on the lower surface |
| $K$ | II B [Eq. (13)] | $cm^3s^{-1}$ | Two-body recombination rate coefficient |
| $K_o,K_p$ | II B [Eq. (16)] | $cm^2s^{-1}$ | Parameterization of two-body rate constants |
| $K_s$ | II B | $cm^2s^{-1}$ | Any two-body surface recombination rate constant |
| $K_{\beta\gamma}$ | II B [Eq. (14)] | $cm^2s^{-1}$ | A specific two-body recombination rate constant |
| $L$ | II E [Eq. (32)] | $cm^6s^{-1}$ | Three-body recombination rate coefficient |
| $L_g$ | II E [Eq. (29)] | $cm^6s^{-1}$ | $L$ in the gas |
| $L_s$ | II E [Eq. (30)] | $cm^4s^{-1}$ | $L$ on the surface |
| $n_a,n_b$ | II A | $cm^{-3}$ | Densities of the $a$ and $b$ states |
| $n_c,n_d$ | II A | $cm^{-3}$ | Densities of the $c$ and $d$ states |
| $n$ | | $cm^{-3}$ | Total density |
| $\dot{n}$ | II B | $cm^{-3}s^{-1}$ | A contribution to the recombination rate |
| $N^{\alpha\beta\gamma;\theta}$ | II E [Eq. (28)] | | Products of a three-body recombination |
| $N^d$ | II E | | Probability of spin-flip during a dipole-dipole recombination |
| $R_K$ | V B 2 | $K\,s\,cm^2erg^{-1}$ | Kapitza resistance of He-Cu interface |
| $R_{gl}$ | V B 2 | $K\,s\,cm^2erg^{-1}$ | Thermal boundary resistance at H-He interface |
| $s(T)$ | V B 1 | | Sticking probability at temperature $T$ |
| $T$ | | K | Sample temperature |

| Symbol | Section | Units | Meaning |
|---|---|---|---|
| $T_g$ | V B 1 | K | Gas temperature |
| $T_s$ | V B 1 | K | Surface temperature |
| $V$ | II B | $cm^3$ | Sample volume |
| $W_g^{ex}$ | II E [Eq. (25)] | $s^{-1}$ | Three-body exchange rate per atom |
| $W_g^d$ | II E [Eq. (26)] | $s^{-1}$ | Three-body dipole-dipole event rate per atom |
| $w$ | V B 2 | cm | Height of the sample cell |
| $X$ | VI C | | $^3$He concentration |


*Present address: Texas Instruments, Dallas, Texas 75243.

[1]I. F. Silvera and J. T. M. Walraven, Phys. Rev. Lett. **44**, 164 (1980).

[2]R. W. Cline, T. J. Greytak, D. Kleppner, and D. A. Smith, J. Phys. (Paris), Colloq. **41**, C7-151 (1980), and R. W. Cline, D. A. Smith, T. J. Greytak, and D. Kleppner, Phys. Rev. Lett. **45**, 2117 (1980).

[3]I. F. Silvera and J. T. M. Walraven, J. Phys. (Paris), Colloq. **41**, C7-137 (1980); J. T. M. Walraven, I. F. Silvera, and A. P. M. Matthey, Phys. Rev. Lett. **45**, 449 (1980).

[4]M. Morrow, R. Jochemsen, A. J. Berlinsky, and W. N. Hardy, Phys. Rev. Lett. **46**, 195 (1981), and **47**, 455 (1981).

[5]A. P. M. Matthey, J. T. M. Walraven, and I. F. Silvera, Phys. Rev. Lett. **46**, 668 (1981).

[6]R. W. Cline, T. J. Greytak, and D. Kleppner, Phys. Rev. Lett. **47**, 1195 (1981).

[7]B. W. Statt and A. J. Berlinsky, Phys. Rev. Lett. **45**, 2105 (1980).

[8]Yu. Kagan, I. A. Vartanyantz, and G. V. Shlyapnikov, Zh. Eksp. Teor. Fiz., **81**, 1113 (1981) [Sov. Phys.—JETP **54**, 590 (1981)].

[9]R. Sprik, J. T. M. Walraven, and I. F. Silvera, Phys. Rev. Lett. **51**, 479 (1983), and **51**, 942 (1983).

[10]H. F. Hess, D. A. Bell, G. P. Kochanski, R. W. Cline, D. Kleppner, and T. J. Greytak, Phys. Rev. Lett. **51**, 483 (1983).

[11]T. J. Greytak and D. Kleppner, *New Trends in Atomic Physics,* Les Houches Summer School, 1982, edited by G. Greenberg and R. Stora (North-Holland, Amsterdam, 1984), p. 1125.

[12]H. F. Hess, D. A. Bell, G. P. Kochanski, D. Kleppner, and T. J. Greytak, Phys. Rev. Lett. **52**, 1520 (1984).

[13]D. A. Bell, G. P. Kochanski, L. Pollack, H. F. Hess, D. Kleppner, and T. J. Greytak, in *Proceedings of the 17th International Conference on Low Temperature Physics,* edited by U. Eckern, A. Schmid, W. Weber, and H. Wuhl (North-Holland, Amsterdam, 1984), p. 449.

[14]D. A. Bell, G. P. Kochanski, D. Kleppner, and T. J. Greytak, in *Proceedings of the 17th International Conference on Low Temperature Physics,* Ref. 13, p. 541.

[15]This value of $K_s$ is about 10% higher than that reported in Ref. 6 due to an improved estimate of the effective area-to-volume ratio of the cell.

[16]B. Yurke, J. S. Denker, B. R. Johnson, N. Bigelow, L. P. Levy, D. M. Lee, and J. H. Freed, Phys. Rev. Lett. **50**, 1137 (1983).

[17]B. W. Statt, A. J. Berlinsky, and W. N. Hardy, Phys. Rev. B **31**, 3169 (1985).

[18]$\gamma$ was determined from a careful analysis of how the pressure decayed as a function of time in an apparatus similar to that of Ref. 6 except for a threefold increase in area-to-volume ratio.

[19]R. Sprik, J. T. M. Walraven, G. H. van Yperen, and I. F. Silvera, Phys. Rev. Lett. **49**, 153 (1982).

[20]G. H. van Yperen, I. F. Silvera, J. T. M. Walraven, J. Berkhout, and J. G. Brisson, Phys. Rev. Lett. **50**, 53 (1983).

[21]J. M. Greben, A. W. Thomas, and A. J. Berlinsky, Can. J. Phys. **59**, 945 (1981).

[22]A. Lagendijk, I. F. Silvera, and B. J. Verhaar, Phys. Rev. B **33**, 626 (1986).

[23]J. P. H. W. van den Eijnde, dissertation, Eindhoven University of Technology, The Netherlands, 1984 (unpublished).

[24]A. Lagendijk, Phys. Rev. B **25**, 2054 (1982).

[25]A. E. Ruckenstein and E. D. Siggia, Phys. Rev. B **25**, 6031 (1982).

[26]B. W. Statt, Phys. Rev. B **25**, 6035 (1982).

[27]R. M. C. Ahn, J. P. H. W. van den Eijnde, C. J. Reuver, B. J. Verhaar, and I. F. Silvera, Phys. Rev. B **26**, 452 (1982).

[28]J. P. H. W. van den Eijnde, C. J. Reuver, and B. J. Verhaar, Phys. Rev. B **28**, 6309 (1983).

[29]E. D. Siggia and A. E. Ruckenstein, Phys. Rev. B **23**, 3580 (1981).

[30]Yu. Kagan, G. V. Shlyapnikov, I. A. Vartanyantz, and N. A. Glukhov, Pis'ma Zh. Eksp. Teor. Fiz. **35**, 386 (1982) [JETP Lett. **35**, 477 (1982)].

[31]L. P. H. de Goey, J. P. J. Driessen, B. J. Verhaar, and J. T. M. Walraven, Phys. Rev. Lett. **53**, 1919 (1984). The values calculated in this reference are what we would refer to as $2C^d$; they are represented by $L$, a symbol which we use to refer to the measurable three-body rate coefficient defined by Eq. (34), that is $L \approx 2(1+N^d)C^d$.

[32]Du Pont Co., Wilmington, Delaware 19898.

[33]J. Wilks, *The Properties of Liquid and Solid Helium* (Oxford, New York, 1967).

[34]Acheson Colloids Co., Port Huron, Michigan 48060.

[35]B. Dodson, T. Low, and J. Mochel, Rev. Sci. Instrum. **48**, 290 (1977).

[36]D. S. Greywall and P. A. Busch, J. Low Temp. Phys. **46**, 451 (1982).

[37]C. T. Van Degrift, Rev. Sci. Instrum. **46**, 599 (1975); C. T. Van Degrift and C. P. Love, Rev. Sci. Instrum. **52**, 712 (1981).

[38]T. Tommila, S. Jaakkola, M. Krusius, K. Salonen, and E. Tjukanov, in *Proceedings of the 17th International Conference on Low Temperature Physics,* Ref. 13, p. 453; Phys. Rev. Lett. **56**, 941 (1986).

[39]Yu. Kagan, G. V. Shlyapnikov, I. A. Vartanyantz, Phys. Lett. **101A**, 27 (1984).

[40]See Eq. (1) in Ref. 10.

[41]I. B. Mantz and D. O. Edwards, Phys. Rev. B **20**, 4518 (1979).

[42]I. F. Silvera and V. V. Goldman, Phys. Rev. Lett. **45**, 915 (1980); V. V. Goldman and I. F. Silvera, Physica **107B&C**, 515 (1981).

[43]D. S. Zimmerman and A. J. Berlinsky, Can. J. Phys. **61**, 508 (1983).

[44]A. C. Anderson, J. I. Connolly, and J. C. Wheatley, Phys. Rev. **135**, A910 (1964).
[45]S. C. Saxena and R. K. Joshi, *Thermal Accommodation and Adsorption Coefficients of Gases* (McGraw-Hill, New York, 1981).
[46]R. Jochemsen, M. Morrow, A. J. Berlinsky, and W. N. Hardy, Phys. Rev. Lett. **47**, 852 (1981).
[47]K. T. Salonen, I. F. Silvera, J. T. M. Walraven, and G. H. van Yperen, Phys. Rev. B **25**, 6001 (1982).
[48]K. Salonen, S. Jaakkola, M. Karhunen, E. Tjukanov, and T. Tommila, *Proceedings of the 17th International Conference on Low Temperature Physics,* Ref. 13, p. 543.
[49]B. Castaing and M. Papoular, J. Phys. (Paris) Lett. **44**, L-537 (1983).
[50]Yu. Kagan, G. V. Shlyapnikov, and I. A. Vartanyantz, Phys. Lett. **101A**, 27 (1984).
[51]V. V. Goldman, Phys. Rev. Lett. **56**, 612 (1986).
[52]C. Lhuiller, J. Phys. (Paris) **44**, 1 (1983).
[53]P. J. Huber, *Robust Statistics* (Wiley, New York, 1981).
[54]D. W. Marquardt, J. Soc. Ind. Appl. Math **11**, 431 (1963).
[55]J. Stoer and R. Bulirsch, *Introduction to Numerical Analysis,* translated by R. Bartels, W. Gautschi, and C. Witzgall (Springer-Verlag, New York, 1980), Sec. 5.4.
[56]M. W. Reynolds, I. Shinkoda, W. N. Hardy, A. J. Berlinsky, F. Bridges, and B. W. Statt, Phys. Rev. B **31**, 7503 (1985).
[57]R. Sprik, J. T. M. Walraven, and I. F. Silvera, Phys. Rev. B **32**, 5668 (1985).
[58]A. Lagendijk, G. H. Van Yperen, and J. T. M. Walraven, J. Phys. (Paris) Lett. **45**, L-929 (1984).
[59]G. H. Van Yperen, A. P. M. Matthey, J. T. M. Walraven, and I. F. Silvera, Phys. Rev. Lett. **47**, 800 (1981).
[60]D. O. Edwards and W. F. Saam, Prog. Low Temp. Phys. VIII A, 283 (1978).
[61]M. Morrow, Ph.D. dissertation, University of British Columbia, 1983 (unpublished).
[62]J. Crank, *The Mathematics of Diffusion* (Clarendon, Oxford, 1956), Eq. (4.18).
[63]M. Morrow and A. J. Berlinsky, Can. J. Phys. **61**, 1042 (1983).